Article

mRNA vaccine-elicited antibodies to SARS-CoV-2 and circulating variants

https://doi.org/10.1038/s41586-021-03324-6

Received: 15 January 2021

Accepted: 3 February 2021

Published online: 10 February 2021

Check for updates

Zijun Wang[1,10], Fabian Schmidt[2,10], Yiska Weisblum[2,10], Frauke Muecksch[2,10], Christopher O. Barnes[3,10], Shlomo Finkin[1,10], Dennis Schaefer-Babajew[1,10], Melissa Cipolla[1,10], Christian Gaebler[1,10], Jenna A. Lieberman[4,10], Thiago Y. Oliveira[1], Zhi Yang[3], Morgan E. Abernathy[3], Kathryn E. Huey-Tubman[3], Arlene Hurley[5], Martina Turroja[1], Kamille A. West[6], Kristie Gordon[1], Katrina G. Millard[1], Victor Ramos[1], Justin Da Silva[2], Jianliang Xu[4], Robert A. Colbert[7], Roshni Patel[1], Juan Dizon[1], Cecille Unson-O'Brien[1], Irina Shimeliovich[1], Anna Gazumyan[1], Marina Caskey[1], Pamela J. Bjorkman[3]✉, Rafael Casellas[4,8]✉, Theodora Hatziioannou[2]✉, Paul D. Bieniasz[2,9]✉ & Michel C. Nussenzweig[1,9]✉

Here we report on the antibody and memory B cell responses of a cohort of 20 volunteers who received the Moderna (mRNA-1273) or Pfizer–BioNTech (BNT162b2) vaccine against SARS-CoV-2[1–4]. Eight weeks after the second injection of vaccine, volunteers showed high levels of IgM and IgG anti-SARS-CoV-2 spike protein (S) and receptor-binding-domain (RBD) binding titre. Moreover, the plasma neutralizing activity and relative numbers of RBD-specific memory B cells of vaccinated volunteers were equivalent to those of individuals who had recovered from natural infection[5,6]. However, activity against SARS-CoV-2 variants that encode E484K-, N501Y- or K417N/E484K/N501-mutant S was reduced by a small—but significant—margin. The monoclonal antibodies elicited by the vaccines potently neutralize SARS-CoV-2, and target a number of different RBD epitopes in common with monoclonal antibodies isolated from infected donors[5–8]. However, neutralization by 14 of the 17 most-potent monoclonal antibodies that we tested was reduced or abolished by the K417N, E484K or N501Y mutation. Notably, these mutations were selected when we cultured recombinant vesicular stomatitis virus expressing SARS-CoV-2 S in the presence of the monoclonal antibodies elicited by the vaccines. Together, these results suggest that the monoclonal antibodies in clinical use should be tested against newly arising variants, and that mRNA vaccines may need to be updated periodically to avoid a potential loss of clinical efficacy.

Between 19 October 2020 and 15 January 2021, we recruited 20 volunteers who received 2 doses of the Moderna (n = 14) or Pfizer–BioNTech mRNA (n = 6) vaccines for blood donation. The volunteers ranged from 29 to 69 years old (median 43); 12 (60%) were men and 8 (40%) women. Sixteen participants identified as Caucasian, two identified as Hispanic, one identified as African American and one identified as Asian. The time from the second vaccination to sample collection varied between 3 and 14 weeks (average of 8 weeks). None of the volunteers had a history of previous infection with SARS-CoV-2, and none experienced serious adverse events after vaccination (Supplementary Table 1).

Plasma activity against SARS-CoV-2 after vaccination

Plasma IgM, IgG and IgA responses to SARS-CoV-2 S and RBD were measured by enzyme-linked immunosorbent assay (ELISA)[5,6]. All of the individuals we tested showed a reactivity to S and RBD that was significantly higher compared to historic controls (from before COVID-19) (Extended Data Fig. 1a–f). As might be expected, levels of anti-S and anti-RBD IgG were higher than those of IgM or IgA. Moreover, there was a strong positive correlation between the anti-RBD and anti-S response in all three of the immunoglobulin isotypes we measured (Extended Data Fig. 1g–i). Consistent with previous reports[2,9,10], levels

[1]Laboratory of Molecular Immunology, The Rockefeller University, New York, NY, USA. [2]Laboratory of Retrovirology, The Rockefeller University, New York, NY, USA. [3]Division of Biology and Biological Engineering, California Institute of Technology, Pasadena, CA, USA. [4]Lymphocyte Nuclear Biology, National Institute of Arthritis and Musculoskeletal and Skin Diseases, National Institutes of Health, Bethesda, MD, USA. [5]Hospital Program Direction, The Rockefeller University, New York, NY, USA. [6]Department of Transfusion Medicine, National Institutes of Health Clinical Center, Bethesda, MD, USA. [7]Pediatric Translational Research Branch and Office of the Clinical Director, National Institute of Arthritis and Musculoskeletal and Skin Diseases, National Institutes of Health, Bethesda, MD, USA. [8]The NIH Regulome Project, National Institutes of Health, Bethesda, MD, USA. [9]Howard Hughes Medical Institute, The Rockefeller University, New York, NY, USA. [10]These authors contributed equally: Zijun Wang, Fabian Schmidt, Yiska Weisblum, Frauke Muecksch, Christopher O. Barnes, Shlomo Finkin, Dennis Schaefer-Babajew, Melissa Cipolla, Christian Gaebler, Jenna A. Lieberman. ✉e-mail: bjorkman@caltech.edu; rafael.casellas@nih.gov; thatziio@rockefeller.edu; pbieniasz@rockefeller.edu; nussen@rockefeller.edu

of IgG and IgM were significantly higher in the vaccinated group than in a cohort of patients who had recovered from COVID-19 (assayed at 1.3 and 6.2 months after infection), whereas IgA levels were similar between the two groups (Extended Data Fig. 1j–l).

We determined plasma neutralizing activity using human immunodeficiency virus-1 (HIV-1) pseudotyped with SARS-CoV-2 S[5,6,11]. Consistent with previous reports[2,9,10], there was a broad range of plasma neutralizing activity at 3–14 weeks after the second dose of vaccine; this range was similar to that elicited by natural infection in the cohort of patients who had recovered from COVID-19 after 1.3 months, and greater than the activity at 6.2 months after infection (Fig. 1a, Supplementary Table 1). There was no significant difference in neutralizing activity between the Moderna and the Pfizer–BioNTech vaccines (Fig. 1b). Whereas antibody titres in the cohort of patients who had recovered from COVID-19 tended to correlate with severity and length of time of infection, additional sampling would be required to understand the correlates of the magnitude of the vaccine response. As expected, plasma neutralizing activity was directly correlated with anti-S and anti-RBD binding titres in ELISAs[5,6] (Fig. 1c, d, Extended Data Fig. 2a–d). Finally, RBD and S binding, and neutralizing activities, were directly correlated with the time between the first dose of vaccine and blood donation: levels of all three measurements were significantly reduced with time[12] (Fig. 1e–g, Extended Data Fig. 2e–h). However, this, and other small studies[2,12], cannot accurately predict the half-life of the neutralizing response. Larger numbers of individuals in diverse cohorts will be needed to determine the precise half-life of the neutralizing response elicited by the vaccine.

To determine whether plasma from vaccinated individuals can neutralize circulating SARS-CoV-2 variants of concern and mutants that arise in vitro under antibody pressure[13,14], we tested plasma from vaccinated individuals against a panel of ten mutant pseudotype viruses, including the recently reported N501Y (B1.1.7 variant), K417N, E484K and K417N/E484K/N501Y (501Y.V2 variant) mutations of the RBD[15–20]. Plasma from vaccinated individuals was significantly less effective in neutralizing the HIV-1 virus pseudotyped with particular mutants of the SARS-CoV-2 S (Fig. 1h, i, Extended Data Fig. 2j). In the plasma we tested, there was a one- to threefold decrease in neutralizing activity against E484K, N501Y and K417N/E484K/N501Y ($P = 0.0033$, $P = 0.0002$ and $P < 0.0001$, respectively) (Fig. 1h, i). Similarly, plasma obtained from the cohort of patients who had recovered from COVID-19 at 1.3 and 6.2 months after infection was 0.5- to 29-fold and 0.5- to 20.2-fold less effective in neutralizing the K417N/E484K/N501Y mutant ($P = 0.001$ and $P < 0.0001$, respectively) (Fig. 1j, Supplementary Table 2). We conclude that the plasma neutralizing activity elicited by mRNA vaccination or natural infection is variably, but significantly, less effective against pseudoviruses that carry RBD mutations that are found in emerging variants of SARS-CoV-2.

Vaccine-elicited monoclonal antibodies

Although circulating antibodies derived from plasma cells wane over time, long-lived immune memory can persist in expanded clones of memory B cells[5,21]. We used flow cytometry to enumerate the circulating SARS-CoV-2 RBD-specific memory B cells elicited by mRNA immunization[5,6] (Fig. 2a, Extended Data Fig. 3a, b). We focused on the RBD because it is the target of the majority of the more-potent SARS-CoV-2 neutralizing antibodies discovered to date[22–27]. Notably, the percentage of RBD-binding memory B cells in vaccinated individuals was significantly greater than in naturally infected individuals assayed after 1.3 months, but similar to the same individuals assayed after 6.2 months (Fig. 2b). The percentage of RBD-binding memory B cells in vaccinated individuals was not correlated with the time after vaccination (Extended Data Fig. 3c). Thus, mRNA vaccination elicits a robust SARS-CoV-2 RBD-specific B cell memory response that resembles that following natural infection.

To examine the nature of the antibodies produced by memory B cells in response to vaccination, we obtained 1,409 paired antibody heavy and light chains from RBD-binding single B cells from 14 individuals (10 who had received the Moderna vaccine, and 4 who had received the Pfizer–BioNTech vaccine) (Supplementary Table 3). Expanded clones of cells comprised 4–50% of the overall RBD-binding memory B cell compartment (Fig. 2c, d, Extended Data Fig. 3d). Similar to natural infection, *IGHV3-53* and *IGHV3-30*, as well as some IGLV genes, were significantly over-represented in the RBD-binding memory B cell compartment of vaccinated individuals (Fig. 2e, Extended Data Fig. 4a). In addition, antibodies that share the same combination of IGHV and IGLV genes in vaccinated individuals comprised 39% of all the clonal sequences (Extended Data Fig. 4b), and 59% when combined with naturally infected individuals[5,6] (Fig. 2f); some of these antibodies were nearly identical (Supplementary Tables 3, 4). The number of nucleotide mutations in the V gene in vaccinated individuals is greater than in naturally infected individuals assayed after 1.3 months, but lower than that in the same individuals assayed after 6.2 months (Fig. 2g, Extended Data Fig. 5a). The length of the IgH CDR3 was similar in both naturally infected and vaccinated individuals, and hydrophobicity was below average[28] (Fig. 2h, Extended Data Fig. 5a, b). Thus, the IgG memory response is similar in individuals who received the Pfizer–BioNTech and Moderna vaccines, and both of these groups are rich in recurrent and clonally expanded antibody sequences.

One hundred and twenty-seven representative antibodies from eight vaccinated individuals were expressed and tested for reactivity to the RBD (Supplementary Table 5). The antibodies included: (1) 76 that were randomly selected from those that appeared only once, and (2) 51 representatives of expanded clones. Of the antibodies tested, 98% (124 out of 127) bound to the RBD, which indicates that single-cell sorting by flow cytometry efficiently identified B cells that produce anti-RBD antibodies (Extended Data Fig. 6a–c, Supplementary Table 5). In anti-RBD ELISAs, the mean half-maximal effective concentration was higher than that observed for antibodies obtained from naturally infected individuals after 6.2 months but not significantly different from antibodies obtained 1.3 months after infection[5,6] (Extended Data Fig. 6a, Supplementary Table 5). To examine memory B cell antibodies for binding to circulating SARS-CoV-2 variants and antibody-resistant mutants, we performed ELISAs using mutant RBDs[7,8,13,16,29,30]. Twenty-two (26%) of the 84 antibodies we tested showed at least fivefold-decreased binding to at least one of the mutant RBDs (Extended Data Fig. 6d–n, Supplementary Table 5).

We used SARS-CoV-2 S pseudotyped viruses to measure the neutralizing activity of all 127 antibodies[5,6,11] (Fig. 3a, Supplementary Table 5). Consistent with the plasma neutralization results, the geometric mean neutralization half-maximal inhibitory concentration (IC_{50}) values of the antibodies of individuals vaccinated with the Pfizer–BioNTech or Moderna vaccine were not significantly different from each other, or to antibody collections obtained from naturally infected individuals at 1.3 or 6.2 months after infection[5,6] (Fig. 3a).

To examine the neutralizing breadth of the monoclonal antibodies and to begin to map their target epitopes, we tested 17 of the most potent antibodies (Supplementary Table 6)—8 of which carried IgHV3-53—against a panel of 12 SARS-CoV-2 variants: A475V is resistant to class-1 antibodies (structurally defined as previously described[7]); E484K and Q493R are resistant to class-2 antibodies[5–8,13,14,31,32]; and R346S, N439K and N440K are resistant to class-3 antibodies[5–7,13,14,32]. In addition, K417N, Y453F, S477R, N501Y and D614G represent circulating variants, some of which have been associated with rapidly increasing case numbers[15,16,20,32–34]. On the basis of their neutralizing activity against the variants, all but three of the antibodies were provisionally assigned to a defined antibody class or a combination (Fig. 3b). As seen in natural infection, a majority of the antibodies tested (9 out of 17) were at least tenfold-less effective against pseudotyped viruses carrying the E484K mutation[5,7,13]. In addition, five of the antibodies were less potent against K417N, and four were less potent against N501Y, by tenfold or more

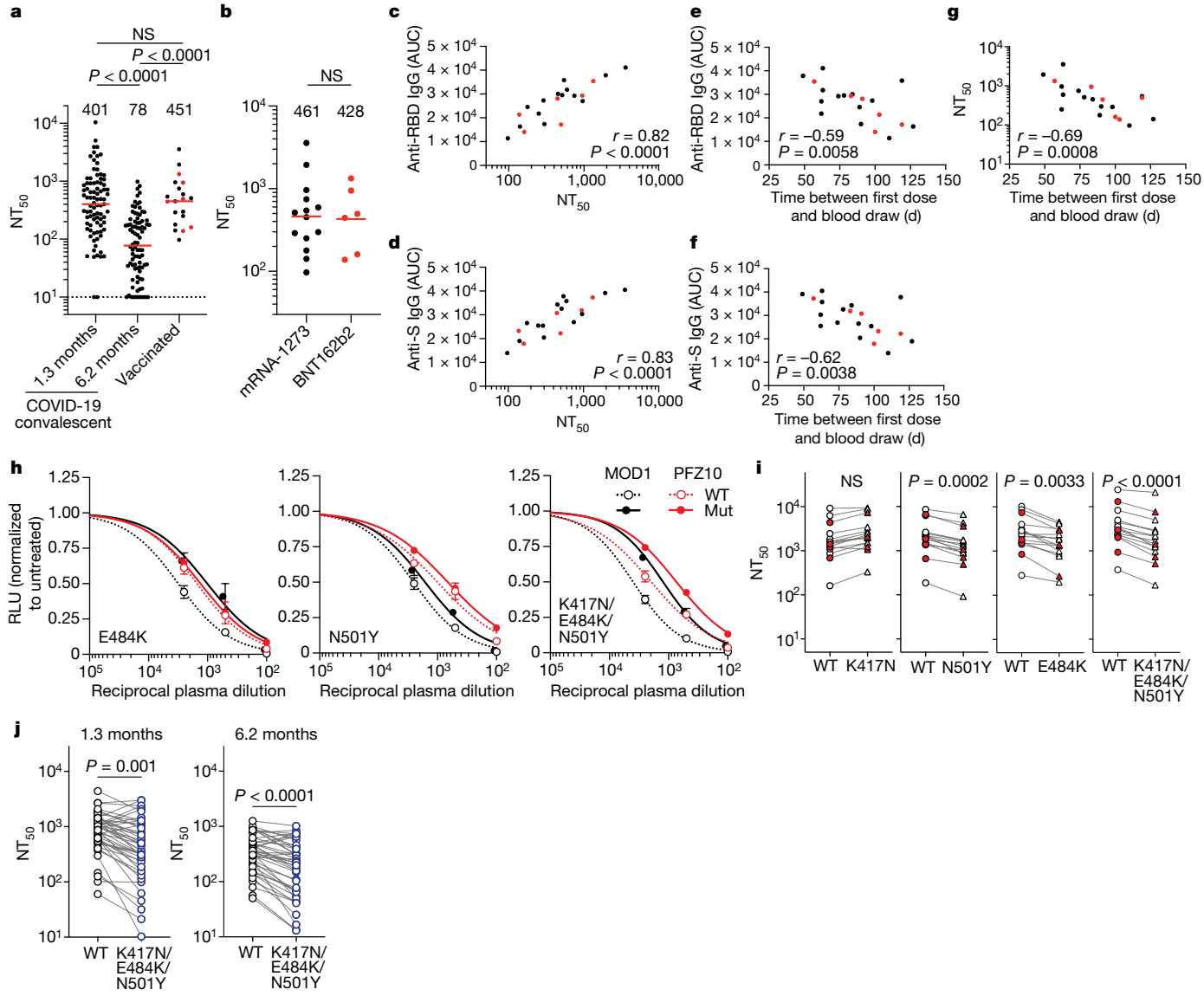

Fig. 1 | Plasma neutralizing activity. a, SARS-CoV-2 pseudovirus neutralization assay. Half-maximal neutralizing titre (NT_{50}) values for plasma obtained from patients who had recovered from COVID-19, measured at 1.3 months[6] and 6.2 months[5] after infection, as well as plasma from vaccinated individuals. NT_{50} values lower than 10 were plotted as 10. Mean of two independent experiments. Red bars and indicated values represent geometric mean NT_{50} values. Statistical significance was determined using the two-tailed Mann–Whitney *U* test. Pre-COVID-19 historical-control plasma was analysed as a negative control and showed no detectable neutralization ($NT_{50} < 10$, not included in panel). NS, not significant. **b**, NT_{50} values for recipients of the Moderna mRNA-1273 (black) and Pfizer–BioNTech BNT162b2 (red) vaccines. Red bars and indicated values represent geometric mean NT_{50} values. Statistical significance was determined using the two-tailed Mann–Whitney *U* test. **c**, Anti-RBD IgG area under the curve (AUC) values (*y* axis) plotted against NT_{50} (*x* axis). **d**, Anti-S IgG AUC (*y* axis) plotted against NT_{50} (*x* axis). **e**, Anti-RBD IgG AUC (*y* axis) plotted against time between first dose and blood draw (*x* axis). **f**, Anti-S IgG AUC (*y* axis) plotted against time between first dose and blood draw (*x* axis). **g**, NT_{50} (*y* axis) plotted against time between first dose and blood draw (*x* axis). The *r* and *P* values for correlations in **c**–**g** were determined by two-tailed Spearman correlation. Individuals who received the Moderna vaccine are shown in black and individuals who received the Pfizer–BioNTech vaccine are in red. **h**, Examples of neutralization assays, comparing the sensitivity of pseudotyped viruses with wild-type (WT) and RBD-mutant (mut) SARS-CoV-2 S to plasma from vaccinated individuals. MOD1 and PFZ10 indicate two representative individuals who received the Moderna and Pfizer–BioNTech vaccine, respectively (Supplementary Table 1). RLU, relative luminescence units. **i**, NT_{50} values for neutralization by plasma from vaccinated individuals ($n = 15$) of pseudotyped viruses with wild-type and the indicated RBD-mutant SARS-CoV-2 S. Individuals vaccinated with the Pfizer–BioNTech vaccine are in red. **j**, NT_{50} values for neutralization by plasma from individuals who had recovered from COVID-19 ($n = 45$) of pseudotyped viruses with wild-type and K417N/E484K/N501Y SARS-CoV-2 S. Statistical significance in **i**, **j** was determined using a one-tailed *t*-test. All experiments were performed a minimum of two times. Pseudotyped viruses containing the E484K mutation and corresponding wild-type controls contain the R683G mutation (Methods).

(Fig. 3b). We obtained similar results with antibodies that are being developed for clinical use (REGN10987, REGN10933, COV2-2196, COV2-2130, C135 and C144) (Extended Data Fig. 7). However, combinations of antibodies remained effective against all of the variants we tested, which confirms the importance of using combinations of antibodies in the clinic (Extended Data Fig. 7). Whether less-potent antibodies show similar degrees of sensitivity to these mutations remains to be determined.

To determine whether antibody-imposed selection pressure could also drive the emergence of resistance mutations in vitro, we cultured a recombinant vesicular stomatitis virus (rVSV)–SARS-CoV-2 virus in the presence of each of 18 neutralizing monoclonal antibodies. All of the

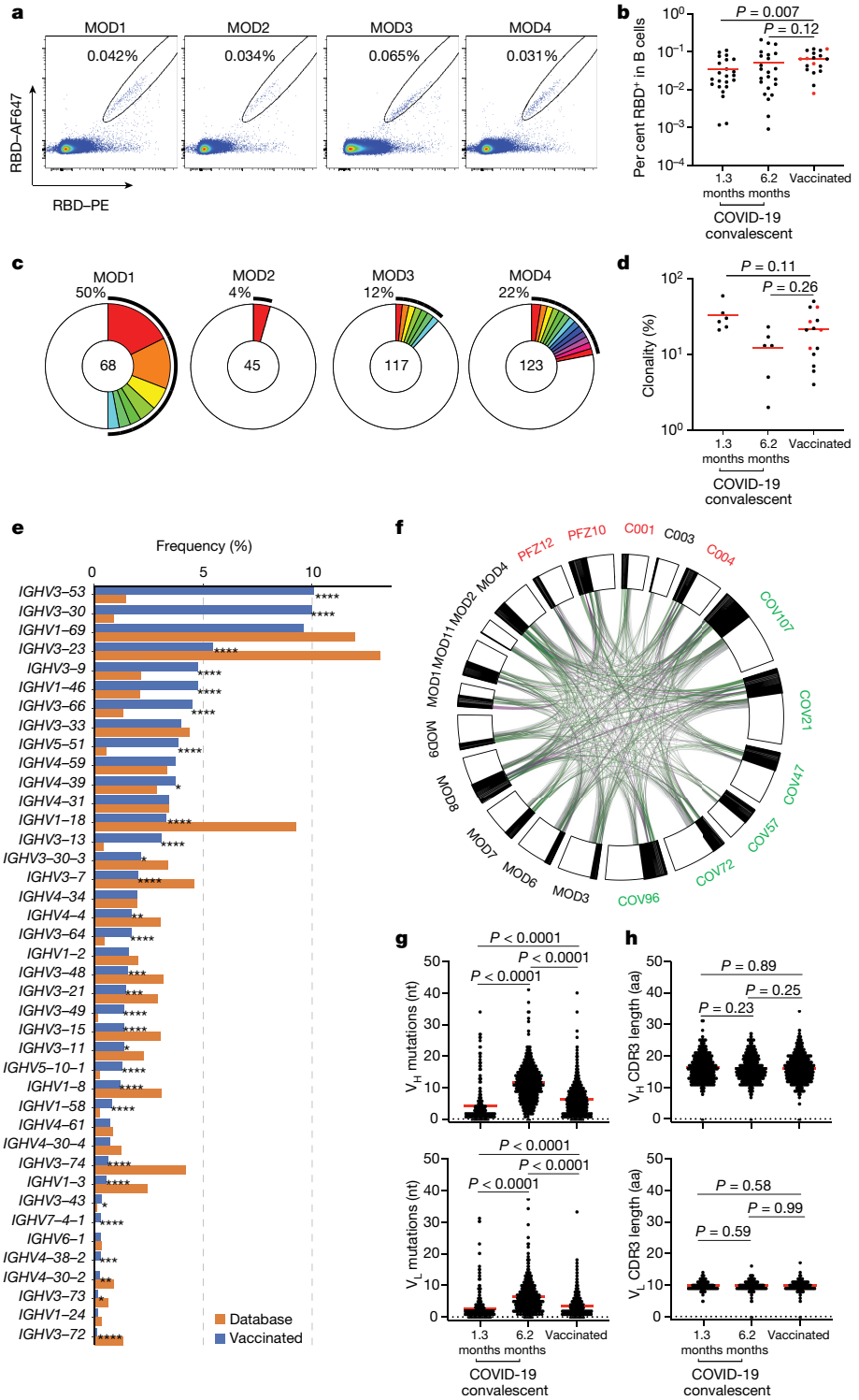

Fig. 2 | Memory B cell antibodies. **a**, Representative flow cytometry plots showing dual AlexaFluor 647–RBD- and PE–RBD-binding B cells for four vaccinated individuals. **b**, As in **a**, dot plot summarizes the percentage of RBD-binding B cells in 19 vaccinated individuals, in comparison to a cohort of naturally infected individuals assayed at 1.3 and 6.2 months after infection[5,6]. Individuals who received the Moderna vaccine are shown in black and individuals who received the Pfizer–BioNTech vaccine are in red. Red horizontal bars indicate mean values. Statistical significance was determined using two-tailed Mann–Whitney *U* tests. **c**, Pie charts show the distribution of antibody sequences from the four individuals in **a**. The number in the inner circle indicates the number of sequences analysed. Pie-slice size is proportional to the number of clonally related sequences. The black outline indicates the frequency of clonally expanded sequences. **d**, As in **c**, graph shows relative clonality among 14 vaccinated individuals. Individuals who received the Moderna vaccine are shown in black and individuals who received the Pfizer–BioNTech vaccine are in red. Red horizontal bars indicate mean values. Statistical significance was determined using two-tailed Mann–Whitney *U* tests. **e**, Graph shows relative abundance of human IGVH genes in data from Sequence Read Archive accession SRP010970 (database) (orange), and vaccinated individuals (blue). A two-sided binomial test was used to compare the frequency distributions. $^{*}P < 0.05$, $^{**}P < 0.01$, $^{***}P < 0.001$, $^{****}P < 0.0001$. **f**, Clonal relationships between sequences from 14 vaccinated individuals (Moderna in black, Pfizer–BioNTech in red) (Supplementary Table 3) and naturally infected individuals[5,6] (green). Interconnecting lines indicate the relationship between antibodies that share V and J gene-segment sequences at both IGH and IGL. Purple, green, and grey lines connect related clones, clones and singles, and singles to each other, respectively. **g**, Number of somatic nucleotide mutations in the IGVH (top) and IGVL (bottom) in antibodies from vaccinated individuals (Supplementary Table 3), compared to those from naturally infected individuals obtained at 1.3 or 6.2 months after infection[5,6]. Statistical significance was determined using two-tailed Mann–Whitney *U* tests. Red horizontal bars indicate mean values. **h**, As in **g**, but for CDR3 length in amino acids (aa).

tested antibodies selected for RBD mutations. Moreover, in all cases, the selected mutations corresponded to residues in the binding sites of their presumptive antibody class (Fig. 3b, c). For example, antibody C627—which was assigned to class 2 on the basis of sensitivity to the E484K mutation—selected for the emergence of the E484K mutation in vitro (Fig. 3c). Notably, six of the antibodies selected for K417N, K417E or K417T, five selected for E484K and three selected for N501Y, N501T or N501H, which coincide with mutations that are present in the circulating B.1.1.17/501Y.V1, B.1.351/501Y.V2 and B1.1.28/501.V3 (P.1) variants that have been associated with rapidly increasing case numbers in particular locales[15,18,19,35].

Cryo-electron microscopy of antibody epitopes

To further characterize antibody epitopes and mechanisms of neutralization, we characterized seven complexes between Fab fragments of monoclonal antibodies and the prefusion, stabilized ectodomain trimer of SARS-CoV-2 S[36] using single-particle cryo-electron microscopy (cryo-EM) (Fig. 4, Supplementary Table 7). Overall resolutions ranged from 5 to 8 Å (Extended Data Fig. 8), and we fit coordinates from S trimer and representative Fab crystal structures by rigid-body docking into the cryo-EM density maps to provide a general assessment of antibody footprints and RBD epitopes. Fab–S complexes exhibited multiple

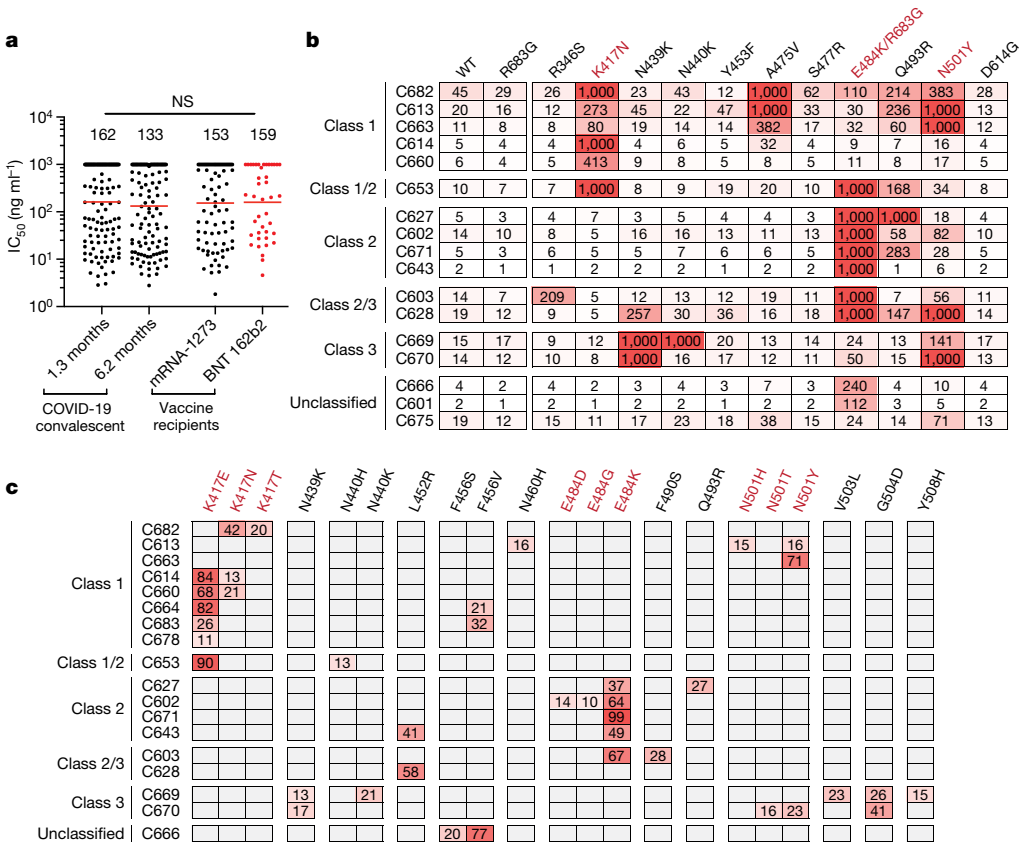

Fig. 3 | Neutralizing activity of anti-SARS-CoV-2 RBD monoclonal antibodies. a, SARS-CoV-2 pseudovirus neutralization assay. IC_{50} values for antibodies cloned from patients who had recovered from COVID-19 measured at 1.3 and 6.2 months[5,6] after infection, as well as antibodies cloned from recipients of the Moderna mRNA-1273 (black) and Pfizer–BioNTech BNT162b2 (red) vaccines. Antibodies with IC_{50} values above 1,000 ng ml^{-1} were plotted as 1,000 ng ml^{-1}. Mean of two independent experiments. Red bars and indicated values represent geometric mean IC_{50} values in ng ml^{-1}. Statistical significance was determined using the two-tailed Mann–Whitney *U* test. Isotype-control antibody was analysed in parallel and showed no detectable neutralization. **b**, IC_{50} values for 17 selected monoclonal antibodies for neutralization of wild-type and the indicated mutant SARS-CoV-2 pseudoviruses. Colour gradient indicates IC_{50} values ranging from 0 (white) to 1,000 ng ml^{-1} (red). **c**, Antibody selection pressure can drive the emergence of S variants in cell culture; the percentage of sequence reads encoding the indicated RBD mutations after a single passage of rVSV–SARS-CoV-2 in the presence of the indicated antibodies is tabulated. Colour gradient indicates the percentage of sequence reads that bear the indicated mutation, ranging from 0 (white) to 100 (red). Positions for which no sequence read was detected are shown in grey. The percentages calculated for a given position are based on all the reads, and not only the reads that include that position. Mutations affecting K417, E484 and N501 are highlighted in **b**, **c**, as they constitute important circulating variants.

RBD-binding orientations that recognized either the 'up' and 'down' RBD conformations (Fig. 4a–j) or solely the 'up' RBD conformation (Fig. 4k–n), consistent with structurally defined antibody classes from natural infection[7] (Fig. 4o). The majority of the monoclonal antibodies that we characterized (6 out of 7) recognized epitopes that included RBD residues involved in ACE2 recognition, which suggests a neutralization mechanism that directly blocks interactions between ACE2 and the RBD. In addition, structurally defined antibody epitopes were consistent with RBD positions that were selected in rVSV–SARS-CoV-2 recombinant virus outgrowth experiments, including residues K417, N439 and N440 (which are in close proximity to one another), E484, and N501 (Fig. 3c, Fig. 4f–j, m, n). Together, these data suggest that functionally similar antibodies are raised during vaccination and natural infection, and that the RBDs of S trimers translated from the mRNA delivered by vaccination adopt both up and down conformations, as observed on structures of trimer ectodomains[7] and trimers on the surface of SARS-CoV-2 virions[37].

Discussion

The mRNA-based SARS-CoV-2 vaccines are safe and effective, and are being deployed globally to prevent infection and disease. The vaccines elicit antibody responses against the RBD (the major target of neutralizing antibodies[22–27]) in a manner that resembles natural infection. Notably, the neutralizing antibodies produced by mRNA vaccination target the same epitopes as those produced by natural infection. Data are consistent with SARS-CoV-2 S trimers translated from the injected RNA adopting a range of different conformations. Moreover, different individuals immunized with the Moderna (mRNA-1273) or Pfizer–BioNTech (BNT162b2) vaccines produce closely related, and nearly identical, antibodies. Whether or not neutralizing antibodies to epitopes other than those involving the RBD are elicited by vaccination remains to be determined.

Human neutralizing monoclonal antibodies to the SARS-CoV-2 RBD can be categorized as belonging to four classes on the basis of their target regions on the RBD[7]. Class-1 and -2 antibodies are among the most potent and also the most abundant antibodies[5,6,22,23,26,38]. These antibodies target epitopes that overlap or are closely associated with RBD residues K417, E484 and N501. They are frequently sensitive to mutation in these residues and select for K417N, E484K and N501Y mutations in SARS-CoV-2 S expression libraries in yeast and VSV[13,16,32]. To avert selection and escape, antibody therapies should be composed of combinations of antibodies that target non-overlapping or highly conserved epitopes[6,13,14,32,39–43].

A number of circulating SARS-CoV-2 variants that have been associated with rapidly increasing case numbers and have particular

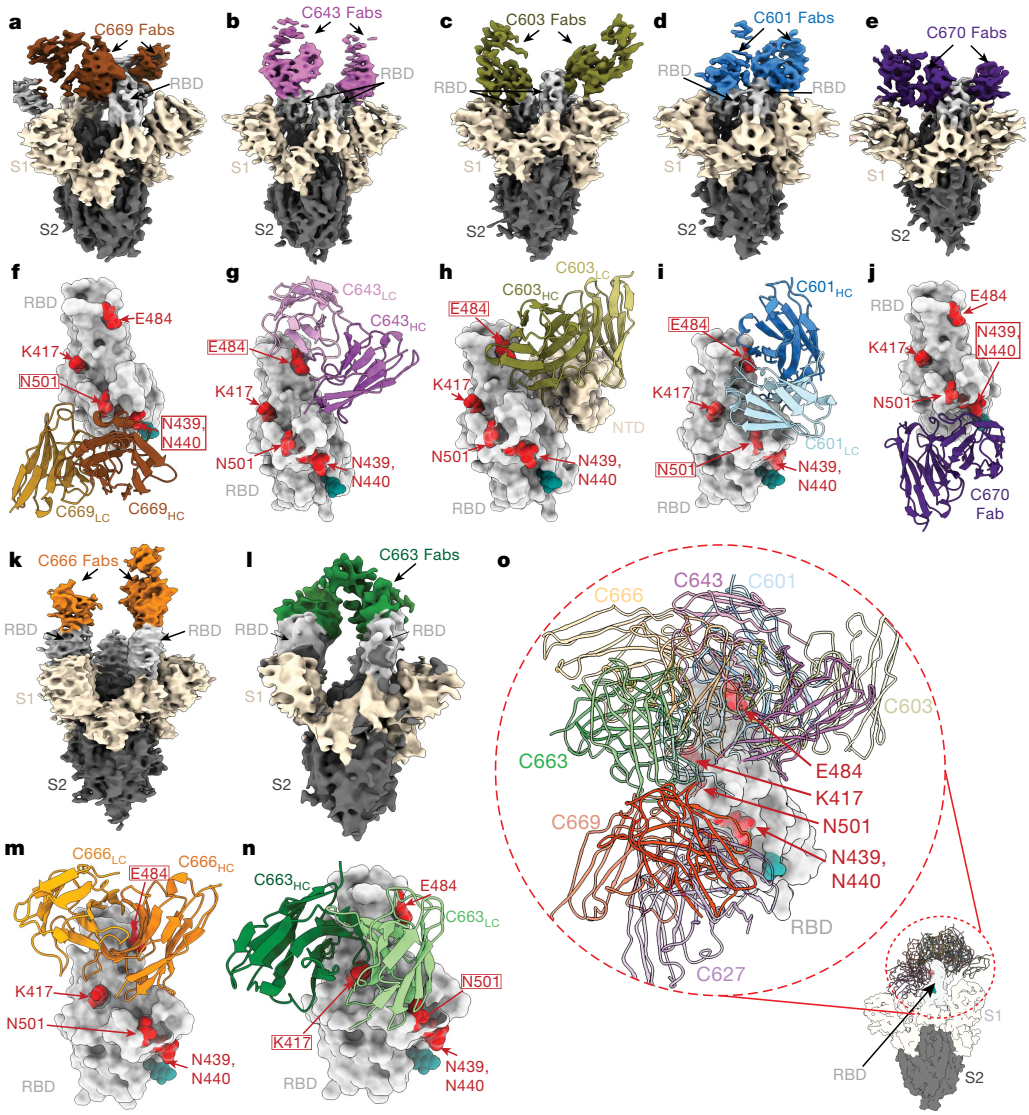

Fig. 4 | Cryo-EM reconstructions of Fab–S complexes. a–**n**, Cryo-EM densities for Fab–S complexes (**a**–**e**, **k**, **l**) and close-up views of antibody footprints on RBDs (**f**–**j**, **m**, **n**) are shown for neutralizing monoclonal antibodies. As expected, owing to Fab interdomain flexibility, cryo-EM densities (**a**–**e**, **k**, **l**) were weak for the Fab C_H–C_L domains. Models of antibody footprints on RBDs (**f**–**j**, **m**, **n**) are presented as Fab V_H–V_L domains (cartoon) complexed with the RBD (surface). To generate models, coordinates of stabilized S trimer (Protein Data Bank code (PDB) 6XKL) and representative Fab fragments (PDB 6XCA or 7K8P) with CDR3 loops removed were fit by rigid-body docking into the cryo-EM density maps. **a**, **f**, C669. **b**, **g**, C643. **c**, **h**, C603. **d**, **i**, C601. **e**, **j**, C670. **k**, **m**, C666. **l**, **n**, C663. RBD residues K417, N439, N440, E484 and N501 are highlighted as red surfaces. The N343 glycan is shown as a teal sphere. HC, heavy chain; LC, light chain. **o**, Composite model illustrating targeted epitopes of RBD-specific neutralizing monoclonal antibodies (shown as V_H–V_L domains in colours from **a**–**l**) elicited from mRNA vaccines.

prevalence in the UK (B.1.1.7/501Y.V1), South Africa (B.1.351/501Y.V2) and Brazil (P.1)[15,18,19,35]. Our experiments indicate that the RBD mutations found in these variants—and potentially others that carry K417N, K417T, E484K and/or N501Y mutations—can reduce the neutralization potency of plasma from vaccinated or naturally infected individuals against SARS-CoV-2 pseudotyped viruses. Although our assays are limited to pseudotyped viruses, there is an excellent correlation between pseudotyped and authentic SARS-CoV-2 neutralization assays[11]. In addition, similar results have previously been reported using plasma from vaccinated and naturally infected individuals, and a variety of different pseudotype and authentic virus assays[16,30,44–48].

The comparatively modest effects of the mutations on viral sensitivity to plasma reflects the polyclonal nature of the neutralizing antibodies in plasma from vaccinated individuals. Nevertheless, emergence of these particular variants is consistent with the dominance of the class-1 and -2 antibody response in infected or vaccinated individuals. We speculate that these mutations emerged in response to immune selection in individuals with nonsterilizing immunity. What the long-term effect of the accumulation of mutations on the SARS-CoV-2 pandemic will be is not known, but the common-cold coronavirus HCoV-229E evolves antigenic variants that are comparatively resistant to the older sera but remain sensitive to contemporaneous sera[49]. Thus, it is possible that these mutations and others that emerge in individuals with suboptimal or waning immunity will erode the effectiveness of natural and vaccine-elicited immunity. The data suggest that SARS-CoV-2 vaccines and antibody therapies may need to be updated and immunity monitored to compensate for viral evolution.

Online content

Any methods, additional references, Nature Research reporting summaries, source data, extended data, supplementary information,

acknowledgements, peer review information; details of author contributions and competing interests; and statements of data and code availability are available at https://doi.org/10.1038/s41586-021-03324-6.

1. Gaebler, C. & Nussenzweig, M. C. All eyes on a hurdle race for a SARS-CoV-2 vaccine. *Nature* **586**, 501–502 (2020).
2. Jackson, L. A. et al. An mRNA vaccine against SARS-CoV-2 – preliminary report. *N. Engl. J. Med.* **383**, 1920–1931 (2020).
3. Krammer, F. SARS-CoV-2 vaccines in development. *Nature* **586**, 516–527 (2020).
4. Polack, F. P. et al. Safety and efficacy of the BNT162b2 mRNA Covid-19 vaccine. *N. Engl. J. Med.* **383**, 2603–2615 (2020).
5. Gaebler, C. et al. Evolution of antibody immunity to SARS-CoV-2. *Nature*, https://doi.org/10.1038/s41586-021-03207-w (2021).
6. Robbiani, D. F. et al. Convergent antibody responses to SARS-CoV-2 in convalescent individuals. *Nature* **584**, 437–442 (2020).
7. Barnes, C. O. et al. SARS-CoV-2 neutralizing antibody structures inform therapeutic strategies. *Nature* **588**, 682–687 (2020).
8. Barnes, C. O. et al. Structures of human antibodies bound to SARS-CoV-2 spike reveal common epitopes and recurrent features of antibodies. *Cell* **182**, 828–842 (2020).
9. Corbett, K. S. et al. Evaluation of the mRNA-1273 vaccine against SARS-CoV-2 in nonhuman primates. *N. Engl. J. Med.* **383**, 1544–1555 (2020).
10. Sahin, U. et al. COVID-19 vaccine BNT162b1 elicits human antibody and T_H1 T cell responses. *Nature* **586**, 594–599 (2020).
11. Schmidt, F. et al. Measuring SARS-CoV-2 neutralizing antibody activity using pseudotyped and chimeric viruses. *J. Exp. Med.* **217**, e20201181 (2020).
12. Widge, A. T. et al. Durability of responses after SARS-CoV-2 mRNA-1273 vaccination. *N. Engl. J. Med.* **384**, 80–82 (2021).
13. Weisblum, Y. et al. Escape from neutralizing antibodies by SARS-CoV-2 spike protein variants. *eLife* **9**, e61312 (2020).
14. Baum, A. et al. Antibody cocktail to SARS-CoV-2 spike protein prevents rapid mutational escape seen with individual antibodies. *Science* **369**, 1014–1018 (2020).
15. Davies, N. G. et al. Estimated transmissibility and severity of novel SARS-CoV-2 variant of concern 202012/01 in England. Preprint at https://doi.org/10.1101/2020.12.24.20248822 (2020).
16. Greaney, A. J. et al. Comprehensive mapping of mutations to the SARS-CoV-2 receptor-binding domain that affect recognition by polyclonal human serum antibodies. Preprint at https://doi.org/10.1101/2020.12.31.425021 (2021).
17. Greaney, A. J. et al. Complete mapping of mutations to the SARS-CoV-2 spike receptor-binding domain that escape antibody recognition. *Cell Host Microbe* **29**, 44–57 (2021).
18. National Institute of Infectious Diseases. Brief report: new variant strain of SARS-CoV-2 identified in travelers from Brazil. https://www.niid.go.jp/niid/en/2019-ncov-e/10108-covid19-33-en.html (2021).
19. Tegally, H. et al. Emergence and rapid spread of a new severe acute respiratory syndrome-related coronavirus 2 (SARS-CoV-2) lineage with multiple spike mutations in South Africa. Preprint at https://doi.org/10.1101/2020.12.21.20248640 (2020).
20. Lauring, A. S. & Hodcroft, E. B. Genetic variants of SARS-CoV-2–what do they mean? *J. Am. Med. Assoc.* **325**, 529–531 (2021).
21. Amanna, I. J., Carlson, N. E. & Slifka, M. K. Duration of humoral immunity to common viral and vaccine antigens. *N. Engl. J. Med.* **357**, 1903–1915 (2007).
22. Brouwer, P. J. M. et al. Potent neutralizing antibodies from COVID-19 patients define multiple targets of vulnerability. *Science* **369**, 643–650 (2020).
23. Cao, Y. et al. Potent neutralizing antibodies against SARS-CoV-2 identified by high-throughput single-cell sequencing of convalescent patients' B cells. *Cell* **182**, 73–84 (2020).
24. Ju, B. et al. Human neutralizing antibodies elicited by SARS-CoV-2 infection. *Nature* **584**, 115–119 (2020).
25. Liu, L. et al. Potent neutralizing antibodies against multiple epitopes on SARS-CoV-2 spike. *Nature* **584**, 450–456 (2020).
26. Rogers, T. F. et al. Isolation of potent SARS-CoV-2 neutralizing antibodies and protection from disease in a small animal model. *Science* **369**, 956–963 (2020).
27. Zost, S. J. et al. Potently neutralizing and protective human antibodies against SARS-CoV-2. *Nature* **584**, 443–449 (2020).
28. Briney, B., Inderbitzin, A., Joyce, C. & Burton, D. R. Commonality despite exceptional diversity in the baseline human antibody repertoire. *Nature* **566**, 393–397 (2019).
29. Andreano, E. et al. SARS-CoV-2 escape *in vitro* from a highly neutralizing COVID-19 convalescent plasma. Preprint at https://doi.org/10.1101/2020.12.28.424451 (2020).
30. Thomson, E. C. et al. Circulating SARS-CoV-2 spike N439K variants maintain fitness while evading antibody-mediated immunity. *Cell*, https://doi.org/10.1016/j.cell.2021.01.037 (2021).
31. Tortorici, M. A. et al. Ultrapotent human antibodies protect against SARS-CoV-2 challenge via multiple mechanisms. *Science* **370**, 950–957 (2020).
32. Starr, T. N. et al. Prospective mapping of viral mutations that escape antibodies used to treat COVID-19. *Science* **371**, 850–854 (2021).
33. Singer, J., Gifford, R., Cotten, M. & Robertson, D. CoV-GLUE: a web application for tracking SARS-CoV-2 genomic variation. Preprint at https://doi.org/10.20944/preprints202006.0225.v1 (2020).
34. Elbe, S. & Buckland-Merrett, G. Data, disease and diplomacy: GISAID's innovative contribution to global health. *Glob Chall.* **1**, 33–46 (2017).
35. Voloch, C. M. et al. Genomic characterization of a novel SARS-CoV-2 lineage from Rio de Janeiro, Brazil. Preprint at https://doi.org/10.1101/2020.12.23.20248598 (2020).
36. Hsieh, C. L. et al. Structure-based design of prefusion-stabilized SARS-CoV-2 spikes. *Science* **369**, 1501–1505 (2020).
37. Ke, Z. et al. Structures and distributions of SARS-CoV-2 spike proteins on intact virions. *Nature* **588**, 498–502 (2020).
38. Piccoli, L. et al. Mapping neutralizing and immunodominant sites on the SARS-CoV-2 spike receptor-binding domain by structure-guided high-resolution serology. *Cell* **183**, 1024–1042 (2020).
39. Schäfer, A. et al. Antibody potency, effector function, and combinations in protection and therapy for SARS-CoV-2 infection in vivo. *J. Exp. Med.* **218**, e20201993 (2021).
40. Mendoza, P. et al. Combination therapy with anti-HIV-1 antibodies maintains viral suppression. *Nature* **561**, 479–484 (2018).
41. Bar-On, Y. et al. Safety and antiviral activity of combination HIV-1 broadly neutralizing antibodies in viremic individuals. *Nat. Med.* **24**, 1701–1707 (2018).
42. Pinto, D. et al. Cross-neutralization of SARS-CoV-2 by a human monoclonal SARS-CoV antibody. *Nature* **583**, 290–295 (2020).
43. Rappazzo, C. G. et al. An engineered antibody with broad protective efficacy in murine models of SARS and COVID-19. Preprint at https://doi.org/10.1101/2020.11.17.385500 (2020).
44. Cele, S. et al. Escape of SARS-CoV-2 501Y.V2 variants from neutralization by convalescent plasma. Preprint at https://doi.org/10.1101/2021.01.26.21250224 (2021).
45. Wu, K. et al. mRNA-1273 vaccine induces neutralizing antibodies against spike mutants from global SARS-CoV-2 variants. Preprint at https://doi.org/10.1101/2021.01.25.427948 (2021).
46. Xie, X. et al. Neutralization of N501Y mutant SARS-CoV-2 by BNT162b2 vaccine-elicited sera. Preprint at https://doi.org/10.1101/2021.01.07.425740 (2021).
47. Wibmer, C. K. et al. SARS-CoV-2 501Y.V2 escapes neutralization by South African COVID-19 donor plasma. Preprint at https://doi.org/10.1101/2021.01.18.427166 (2021).
48. Li, Q. et al. The impact of mutations in SARS-CoV-2 spike on viral infectivity and antigenicity. *Cell* **182**, 1284–1294 (2020).
49. Eguia, R. et al. A human coronavirus evolves antigenically to escape antibody immunity. Preprint at https://doi.org/10.1101/2020.12.17.423313 (2020).

Publisher's note Springer Nature remains neutral with regard to jurisdictional claims in published maps and institutional affiliations.

© The Author(s), under exclusive licence to Springer Nature Limited 2021

Methods

Data reporting

No statistical methods were used to predetermine sample size. The experiments were not randomized and the investigators were not blinded to allocation during experiments and outcome assessment.

Study participants

To isolate and characterize anti-SARS-CoV-2 RBD antibodies from vaccinated individuals, a cohort of 20 individuals that participated in the Moderna or Pfizer–BioNTech phase-3 vaccine clinical trials and did not report previous history of SARS-CoV-2 infection was recruited at the NIH Blood Center and the Rockefeller University Hospital for blood donation. Eligible participants included adults who were at least 18 years of age, with no known heart, lung, kidney disease or bleeding disorders, and no history of HIV-1 or malaria infection. All participants were asymptomatic at the time of the study visit and had received a complete two-dose regimen of one of the mRNA vaccines. Informed consent was obtained from all participants and the study was conducted in accordance with Good Clinical Practice. The study visits and blood draws were reviewed and approved under the National Institutes of Health's Federalwide Assurance (FWA00005897), in accordance with Federal regulations 45 CFR 46 and 21 CFR 5 by the NIH Intramural Research Program IRB committee (IRB no. 99CC0168, 'Collection and Distribution of Blood Components from Healthy Donors for In vitro Research Use') and by the Institutional Review Board of the Rockefeller University (IRB no. DRO-1006, 'Peripheral Blood of Coronavirus Survivors to Identify Virus-Neutralizing Antibodies'). For detailed participant characteristics, see Supplementary Table 1.

Blood sample processing and storage

Samples collected at NIH were drawn from participants at the study visit and processed within 24 h. In brief, whole-blood samples were subjected to Ficoll gradient centrifugation after 1:1 dilution in PBS. Plasma and peripheral blood mononuclear cell (PBMC) samples were obtained through phase separation of plasma layer and Buffy coat phase, respectively. PBMCs were further prepared through centrifugation, red blood cell lysis and washing steps, and stored in CellBanker cell freezing medium (Amsbio). All samples were aliquoted and stored at −80 °C and shipped on dry ice. Before experiments, aliquots of plasma samples were heat-inactivated (56 °C for 1 h) and then stored at 4 °C. PBMCs obtained from samples collected at Rockefeller University were purified as previously reported[5,6] by gradient centrifugation and stored in liquid nitrogen in the presence of FCS and DMSO. Heparinized plasma samples were aliquoted and stored at −20 °C or below. Before experiments, aliquots of plasma samples were heat-inactivated (56 °C for 1 h) and then stored at 4 °C.

ELISAs

ELISAs[50,51] to evaluate antibodies binding to SARS-CoV-2 S (BioHub), RBD and additional mutated RBDs were performed by coating high-binding 96-half-well plates (Corning 3690) with 50 µl per well of a 1 µg ml^{-1} protein solution in PBS overnight at 4 °C. Plates were washed 6 times with washing buffer (1× PBS with 0.05% Tween-20 (Sigma-Aldrich)) and incubated with 170 µl per well blocking buffer (1× PBS with 2% BSA and 0.05% Tween-20 (Sigma)) for 1 h at room temperature. Immediately after blocking, monoclonal antibodies or plasma samples were added in PBS and incubated for 1 h at room temperature. Plasma samples were assayed at a 1:66.6 (Rockefeller University samples) or a 1:33.3 (NIH samples) starting dilution. and 7 additional 3-fold serial dilutions. Monoclonal antibodies were tested at 10 µg ml^{-1} starting concentration, and 10 additional 4-fold serial dilutions. Plates were washed 6 times with washing buffer and then incubated with anti-human IgG, IgM or IgA secondary antibody conjugated to horseradish peroxidase (HRP) (Jackson Immuno Research 109-036-088 109-035-129 and Sigma A0295) in blocking buffer at a 1:5,000 dilution (IgM and IgG) or 1:3,000 dilution (IgA). Plates were developed by addition of the HRP substrate, TMB (Thermo Fisher Scientific) for 10 min (plasma samples) or 4 min (monoclonal antibodies); the developing reaction was then stopped by adding 50 µl 1 M H_2SO_4, and absorbance was measured at 450 nm with an ELISA microplate reader (FluoStar Omega, BMG Labtech) with Omega and Omega MARS software for analysis. For plasma samples, a positive control (plasma from participant COV72[5,6], diluted 66.6-fold and with 7 additional 3-fold serial dilutions in PBS) was added to every assay plate for validation. The average of its signal was used for normalization of all of the other values on the same plate with Excel software before calculating the AUC using Prism v.8.4 (GraphPad). For monoclonal antibodies, the half-maximal effective concentration (EC_{50}) was determined using four-parameter nonlinear regression (GraphPad Prism v.8.4).

Expression of RBD proteins

Mammalian expression vectors encoding the RBDs of SARS-CoV-2 (GenBank MN985325.1; S residues 319–539) and eight additional mutant RBD proteins (E484K, Q493R, R346S, N493K, N440K, V367F, A475V, S477N and V483A) with an N-terminal human IL-2 or Mu phosphatase signal peptide have previously been described[8].

Cells and viruses

We cultured 293T$_{Ace2}$[6], 293T/ACE2.cl22 and HT1080$_{/}$ACE2.cl14 cells[11] in Dulbecco's modified Eagle medium supplemented with 10% fetal bovine serum at 37 °C and 5% CO_2. Cells were periodically tested for contamination with mycoplasma or retroviruses.

rVSV–SARS-CoV-2–GFP chimeric virus stocks were generated by infecting 293T/ACE2.cl22 cells. Supernatant was collected at 1 day after infection, cleared of cellular debris and stored at −80 °C. A plaque purified variant designated rVSV/SARS-CoV-2/GFP$_{2E1}$ that encodes D215G/R683G substitutions was used in these studies[11].

Selection and analysis of antibody-escape mutations

For the selection of monoclonal-antibody-resistant S variants, an rVSV/SARS-CoV-2/GFP$_{2E1}$[11] population containing 10^6 infectious units was incubated with monoclonal antibodies at 10–40 µg ml^{-1} for 1 h at 37 °C. The virus–antibody mixtures were subsequently incubated with 5×10^5 293T/ACE2cl.22 cells in 6-well plates. One day after infection, the medium was replaced with fresh medium containing the equivalent concentration of antibodies. Supernatant was collected 2 days after infection and 150 µl of the cleared supernatant was used to infect cells for passage 2, and 150 µl was subjected to RNA extraction and sequencing.

For identification of putative antibody-resistance mutations, RNA was extracted using NucleoSpin 96 Virus Core Kit (Macherey-Nagel). The RNA was reversed-transcribed using the SuperScript VILO cDNA Synthesis Kit (Thermo Fisher Scientific). KOD Xtreme Hot Start DNA Polymerase (Millipore Sigma) was used for amplification of cDNA using primers flanking the S-encoding sequence. The PCR products were purified and sequenced as previously described[5,13]. In brief, tagmentation reactions were performed using 1 µl diluted cDNA, 0.25 µl Nextera TDE1 Tagment DNA enzyme (catalogue no. 15027865), and 1.25 µl TD Tagment DNA buffer (catalogue no. 15027866; Illumina). Next, the DNA was ligated to unique i5/i7 barcoded primer combinations using the Illumina Nextera XT Index Kit v.2 and KAPA HiFi HotStart ReadyMix (2×; KAPA Biosystems) and purified using AmPure Beads XP (Agencourt), after which the samples were pooled into one library and subjected to paired-end sequencing using Illumina MiSeq Nano 300 V2 cycle kits (Illumina) at a concentration of 12 pM.

For analysis of the sequencing data, the raw paired-end reads were preprocessed to remove trim adaptor sequences and to remove low-quality reads (Phred quality score < 20) using BBDuk. Reads were mapped to the rVSV–SARS-CoV-2–GFP sequence using Geneious Prime (v.2020.1.2). Mutations were annotated using Geneious Prime, with a P value cutoff of 10^{-6}. Because reads have randomly generated ends

and different lengths, the mutations do not necessarily have to occur on the same read: for example, K417N and N501Y might occur on the same read or on different reads. The percentages calculated for position *X* are calculated on the basis of all the reads, and not only the reads that include position *X*.

SARS-CoV-2 pseudotyped reporter virus

A panel of plasmids expressing RBD-mutant SARS-CoV-2 S proteins in the context of pSARS-CoV-2-$S_{\Delta 19}$ (based on NC_045512) have previously been described[13]. Additional substitutions were introduced using PCR primer-mediated mutagenesis or with synthetic gene fragments (IDT) followed by Gibson assembly. The mutants E484K and K417N/E484K/N501Y were constructed in the context of a pSARS-CoV-2-$S_{\Delta 19}$ variant with a mutation in the furin cleavage site (R683G). The NT_{50} and IC_{50} values of these pseudotypes were compared to a wild-type SARS-CoV-2 S sequence carrying R683G in the subsequent analyses, as appropriate.

The generation of SARS-CoV-2 pseudotyped HIV-1 particles was performed as previously described[6]. In brief, 293T cells were transfected with pNL4-3ΔEnv-nanoluc and pSARS-CoV-2-$S_{\Delta 19}$ and pseudotyped virus stocks were collected 48 h after transfection, filtered and stored at −80 °C.

SARS-CoV-2 pseudotype neutralization assays

Plasma or monoclonal antibodies from vaccine recipients were four-fold or fivefold serially diluted and then incubated with SARS-CoV-2 pseudotyped HIV-1 reporter virus for 1 h at 37 °C. The antibody and pseudotyped virus mixture was added to $293T_{Ace2}$ cells[6] (for comparisons of plasma or monoclonal antibodies from individuals who had recovered from COVID-19 and vaccine recipients) or HT1080ACE2.cl14 cells[11] (for analysis of S mutants with plasma or monoclonal antibodies from recipients of vaccines). After 48 h, cells were washed with PBS and lysed with Luciferase Cell Culture Lysis 5× reagent (Promega) and nanoluc luciferase activity in lysates was measured using the Nano-Glo Luciferase Assay System (Promega) with the Glomax Navigator (Promega). Relative luminescence units were normalized to those derived from cells infected with SARS-CoV-2 pseudotyped virus in the absence of plasma or monoclonal antibodies. The NT_{50} and 80% or 90% neutralization titres (NT_{80} or NT_{90}) for plasma, or IC_{50} and 90% inhibitory concentrations (IC_{90}) for monoclonal antibodies, were determined using 4-parameter nonlinear regression (least-squares regression method without weighting; constraints: top = 1, bottom = 0) (GraphPad Prism).

Biotinylation of viral protein for use in flow cytometry

Purified and Avi-tagged SARS-CoV-2 RBD was biotinylated using the Biotin-Protein Ligase-BIRA kit according to manufacturer's instructions (Avidity), as previously described[6]. Ovalbumin (Sigma, A5503-1G) was biotinylated using the EZ-Link Sulfo-NHS-LC-Biotinylation kit according to the manufacturer's instructions (Thermo Fisher Scientific). Biotinylated ovalbumin was conjugated to streptavidin–BV711 (BD Biosciences, 563262) and RBD to streptavidin–PE (BD Biosciences, 554061) and streptavidin–AlexaFluor647 (Biolegend, 405237)[6].

Flow cytometry and single-cell sorting

Single-cell sorting by flow cytometry was performed as previously described[6]. In brief, PBMCs were enriched for B cells by negative selection using a pan-B cell isolation kit according to the manufacturer's instructions (Miltenyi Biotec, 130-101-638). The enriched B cells were incubated in FACS buffer (1× PBS, 2% FCS, 1 mM EDTA) with the following anti-human antibodies (all at 1:200 dilution): anti-CD20–PECy7 (BD Biosciences, 335793), anti-CD3–APC–eFluro 780 (Invitrogen, 47-0037-41), anti-CD8–APC–eFluor 780 (Invitrogen, 47-0086-42), anti-CD16–APC–eFluor 780 (Invitrogen, 47-0168-41), anti-CD14–APC–eFluor 780 (Invitrogen, 47-0149-42), as well as Zombie NIR (BioLegend, 423105) and fluorophore-labelled RBD and ovalbumin (Ova) for 30 min on ice. Single $CD3^-CD8^-CD14^-CD16^-CD20^+Ova^-RBD\text{–}PE^+RBD\text{–}AlexaFluor647^+$ B cells were sorted into individual wells of 96-well plates containing 4 µl of lysis buffer (0.5× PBS, 10 mM DTT, 3,000 units per ml RNasin Ribonuclease Inhibitors (Promega, N2615)) per well using a FACS Aria III and FACSDiva software (Becton Dickinson) for acquisition and FlowJo for analysis. The sorted cells were frozen on dry ice, and then stored at −80 °C or immediately used for subsequent RNA reverse transcription.

Antibody sequencing, cloning and expression

Antibodies were identified and sequenced as previously described[6]. In brief, RNA from single cells was reverse-transcribed (SuperScript III Reverse Transcriptase, Invitrogen, 18080-044) and the cDNA stored at −20 °C or used for subsequent amplification of the variable IGH, IGL and IGK genes by nested PCR and Sanger sequencing. Sequence analysis was performed using MacVector. Amplicons from the first PCR reaction were used as templates for sequence- and ligation-independent cloning into antibody expression vectors. Recombinant monoclonal antibodies and Fabs were produced and purified as previously described[6].

Cryo-EM sample preparation

Expression and purification of SARS-CoV-2 6P stabilized S trimers[36] was conducted as previously described[52]. Purified Fab and S 6P trimer were incubated at a 1.1:1 molar ratio per protomer on ice for 30 min before deposition on a freshly glow-discharged 300 mesh, 1.2/1.3 Quantifoil copper grid. Immediately before 3 µl of complex was applied to the grid, fluorinated octyl-malotiside was added to the Fab–S complex to a final detergent concentration of 0.02% w/v, resulting in a final complex concentration of 3 mg ml^{-1}. Samples were vitrified in 100% liquid ethane using a Mark IV Vitrobot after blotting for 3 s with Whatman no. 1 filter paper at 22 °C and 100% humidity.

Cryo-EM data collection and processing

Data collection and processing followed a similar workflow to that previously described[7]. In brief, micrographs were collected on a Talos Arctica transmission electron microscope (Thermo Fisher Scientific) operating at 200 kV for all Fab–S complexes. Data were collected using SerialEM automated data collection software[53] and movies were recorded with a K3 camera (Gatan). For all datasets, cryo-EM movies were patch-motion-corrected for beam-induced motion including dose-weighting within cryoSPARC v.2.15[54] after binning super-resolution movies. The non-dose-weighted images were used to estimate CTF parameters using cryoSPARC implementation of the Patch CTF job. Particles were picked using Blob picker and extracted, 4× binned and 2D classified. Class averages corresponding to distinct views with secondary structure features were chosen and ab initio models were generated. Three-dimensional classes that showed features of a Fab–S complex were re-extracted, unbinned (0.869 Å per pixel) and homogenously refined with C1 symmetry. Overall resolutions were reported on the basis of gold-standard Fourier shell correlation calculations.

Cryo-EM structure modelling and refinement

Coordinates for initial complexes were generated by docking individual chains from reference structures into cryo-EM density using UCSF Chimera[55] (S trimer, PDB 6KXL; Fab, PDB 6XCA or 7K8P, after trimming CDR3 loops and converting to a polyalanine model). Models were then refined into cryo-EM maps by rigid-body and real-space refinement in Phenix[56]. If the resolution allowed, partial CDR3 loops were built manually in Coot[57] and then refined using real-space refinement in Phenix.

Computational analyses of antibody sequences

Antibody sequences were trimmed based on quality and annotated using Igblastn v.1.14. with IMGT domain delineation system. Annotation was performed systematically using Change-O toolkit v.0.4.540[58]. Heavy and light chains derived from the same cell were paired, and clonotypes were assigned based on their V and J genes using in-house R and Perl scripts (Fig. 2c, f, Extended Data Figs. 3d, 4b). All scripts and

the data used to process antibody sequences are publicly available at https://github.com/stratust/igpipeline.

The frequency distributions of human V genes in anti-SARS-CoV-2 antibodies from this study were compared to 131,284,220 previously generated IgH and IgL sequences[59] and downloaded from cAb-Rep[60], a database of human shared B cell receptor clonotypes (https://cab-rep.c2b2.columbia.edu/). On the basis of the 97 distinct V genes that make up the 4,186 analysed sequences from immunoglobulin repertoire of the 14 participants present in this study, we selected the IgH and IgL sequences from the database that are partially coded by the same V genes and counted them according to the constant region. The frequencies shown in Fig. 2e, Extended Data Fig. 4a are relative to the source and isotype analysed. We used the two-sided binomial test to check whether the number of sequences belonging to a specific IGHV or IGLV gene in the repertoire is different according to the frequency of the same IGV gene in the database. Adjusted *P* values were calculated using the false discovery rate correction. Significant differences are denoted with asterisks.

Nucleotide somatic hypermutation and CDR3 length were determined using in-house R and Perl scripts. For somatic hypermutations, IGHV and IGLV nucleotide sequences were aligned against their closest germlines using Igblastn and the number of differences were considered nucleotide mutations. The average mutations for V genes were calculated by dividing the sum of all nucleotide mutations across all participants by the number of sequences used for the analysis. To calculate the GRAVY scores of hydrophobicity[61] we used Guy H. R. Hydrophobicity scale based on free energy of transfer (kcal mol^{-1})[62] implemented by the R package Peptides (https://journal.r-project.org/archive/2015/RJ-2015-001/RJ-2015-001.pdf). We used 1,405 heavy-chain CDR3 amino acid sequences from this study and 22,654,256 IgH CDR3 sequences from the public database of memory B cell receptor sequences[63]. The two-tailed Wilcoxon nonparametric test was used to test whether there was a difference in the hydrophobicity distribution.

Data presentation

Figures were arranged in Adobe Illustrator 2020.

Reporting summary

Further information on research design is available in the Nature Research Reporting Summary linked to this paper.

Data availability

Data are provided in Supplementary Tables 1–7. The raw sequencing data and computer scripts associated with Fig. 2 have been deposited at https://github.com/stratust/igpipeline. This study also uses data from refs. [59,63], and from PDB 6VYB and6NB6. Cryo-EM maps associated with data reported in this Article have been deposited in the Electron Microscopy Data Bank (EMDB) (https://www.ebi.ac.uk/pdbe/emdb/) under accession codes EMD-23393 (C601–S), EMD-23394 (C603–S), EMD-23395 (C643–S), EMD-23396 (C663–S), EMD-23397 (C666–S), EMD-23398 (C669–S) and EMD-23399 (C670–S).

Code availability

The computer code used to process the antibody sequences is available at https://github.com/stratust/igpipeline.

50. Amanat, F. et al. A serological assay to detect SARS-CoV-2 seroconversion in humans. *Nat. Med.* **26**, 1033–1036 (2020).
51. Grifoni, A. et al. Targets of T cell responses to SARS-CoV-2 coronavirus in humans with COVID-19 disease and unexposed individuals. *Cell* **181**, 1489–1501 (2020).
52. Cohen, A. A. et al. Mosaic nanoparticles elicit cross-reactive immune responses to zoonotic coronaviruses in mice. *Science* **371**, 735–741 (2021).
53. Mastronarde, D. N. Automated electron microscope tomography using robust prediction of specimen movements. *J. Struct. Biol.* **152**, 36–51 (2005).
54. Punjani, A., Rubinstein, J. L., Fleet, D. J. & Brubaker, M. A. cryoSPARC: algorithms for rapid unsupervised cryo-EM structure determination. *Nat. Methods* **14**, 290–296 (2017).
55. Goddard, T. D. et al. UCSF ChimeraX: meeting modern challenges in visualization and analysis. *Protein Sci.* **27**, 14–25 (2018).
56. Terwilliger, T. C., Adams, P. D., Afonine, P. V. & Sobolev, O. V. A fully automatic method yielding initial models from high-resolution cryo-electron microscopy maps. *Nat. Methods* **15**, 905–908 (2018).
57. Emsley, P., Lohkamp, B., Scott, W. G. & Cowtan, K. Features and development of Coot. *Acta Crystallogr. D* **66**, 486–501 (2010).
58. Gupta, N. T. et al. Change-O: a toolkit for analyzing large-scale B cell immunoglobulin repertoire sequencing data. *Bioinformatics* **31**, 3356–3358 (2015).
59. Soto, C. et al. High frequency of shared clonotypes in human B cell receptor repertoires. *Nature* **566**, 398–402 (2019).
60. Guo, Y., Chen, K., Kwong, P. D., Shapiro, L. & Sheng, Z. cAb-Rep: a database of curated antibody repertoires for exploring antibody diversity and predicting antibody prevalence. *Front. Immunol.* **10**, 2365 (2019).
61. Kyte, J. & Doolittle, R. F. A simple method for displaying the hydropathic character of a protein. *J. Mol. Biol.* **157**, 105–132 (1982).
62. Guy, H. R. Amino acid side-chain partition energies and distribution of residues in soluble proteins. *Biophys. J.* **47**, 61–70 (1985).
63. DeWitt, W. S. et al. A public database of memory and naive B-cell receptor sequences. *PLoS ONE* **11**, e0160853 (2016).
64. Rubelt, F. et al. Onset of immune senescence defined by unbiased pyrosequencing of human immunoglobulin mRNA repertoires. *PLoS ONE* **7**, e49774 (2012).
65. Baum, A. et al. REGN-COV2 antibodies prevent and treat SARS-CoV-2 infection in rhesus macaques and hamsters. *Science* **370**, 1110–1115 (2020).
66. Weinreich, D. M. et al. REGN-COV2, a neutralizing antibody cocktail, in outpatients with Covid-19. *N. Engl. J. Med.* **384**, 238–251 (2021).

Acknowledgements We thank all study participants who devoted time to our research; B. Coller, S. Schlesinger and the Rockefeller University Hospital Clinical Research Support Office and nursing staff; C. M. Rice and all members of the M.C.N. laboratory for helpful discussions and M. Jankovic for laboratory support; and J. Vielmetter and the Protein Expression Center in the Beckman Institute at Caltech for expression assistance. Electron microscopy was performed in the Caltech Beckman Institute Resource Center for Transmission Electron Microscopy, and we thank S. Chen and A. Malyutin for technical assistance. This work was supported by NIH grants P01-AI138398-S1 (M.C.N. and P.J.B.) and 2U19AI111825 (M.C.N.); the Caltech Merkin Institute for Translational Research and P50 AI150464-13 (P.J.B.); a George Mason University Fast Grant (P.J.B.); R37-AI64003 to P.D.B.; and R01AI78788 to T.H. C.O.B. is supported by the HHMI Hanna Gray and Burroughs Wellcome PDEP fellowships. C.G. was supported by the Robert S. Wennett Post-Doctoral Fellowship, in part by the National Center for Advancing Translational Sciences (NIH Clinical and Translational Science Award programme, grant UL1 TR001866), and by the Shapiro–Silverberg Fund for the Advancement of Translational Research. P.D.B. and M.C.N. are Howard Hughes Medical Institute Investigators.

Author contributions P.D.B., P.J.B., R.C., T.H., M.C.N., Z.W., F.S., Y.W., F.M., C.O.B., S.F., D.S.-B. and M. Cipolla conceived, designed and analysed the experiments. M. Caskey, C.G., J.A.L., K.A.W. and D.S.-B. designed clinical protocols. Z.W., F.S., Y.W., F.M., C.O.B., S.F., D.S.-B., M. Cipolla, J.D.S., A.G., Z.Y., M.E.A. K.G. and K.E.H.-T. carried out experiments. C.G., M. Caskey, R.A.C., A.H., M.T. and K.G.M. recruited participants and executed clinical protocols. I.S., R.P., J.D., J.X. and C.U.-O. processed clinical samples. T.Y.O. and V.R. performed bioinformatic analysis. R.C., P.D.B., P.J.B., T.H. and M.C.N. wrote the manuscript, with input from all co-authors.

Competing interests The Rockefeller University has filed a provisional patent application in connection with this work, on which Z.W. and M.C.N. are inventors (US patent 63/199, 676).

Additional information

Supplementary information The online version contains supplementary material available at https://doi.org/10.1038/s41586-021-03324-6.

Correspondence and requests for materials should be addressed to P.J.B., R.C., T.H., P.D.B. or M.C.N.

Peer review information *Nature* thanks the anonymous reviewers for their contribution to the peer review of this work.

Reprints and permissions information is available at http://www.nature.com/reprints.

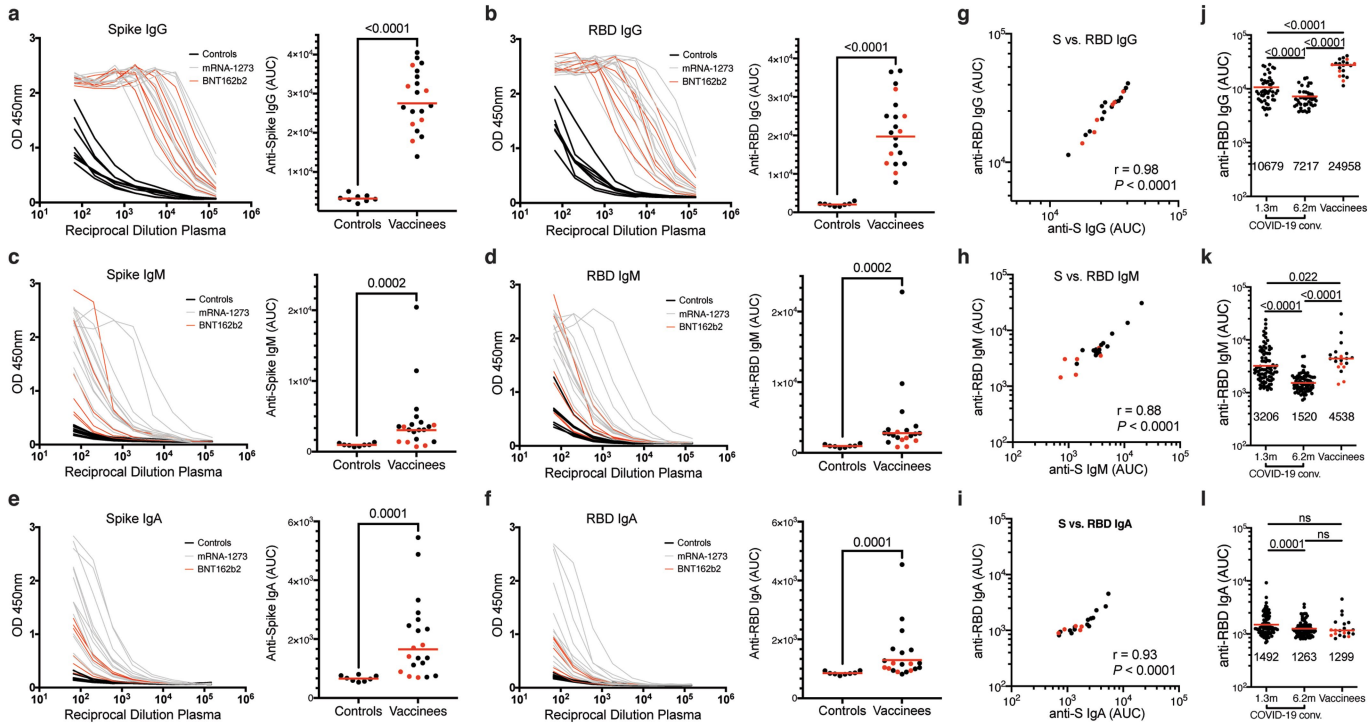

Extended Data Fig. 1 | Plasma antibodies against SARS-CoV-2. a–**f**, Results of ELISAs measuring plasma reactivity to S (**a**, **c**, **e**) and RBD protein (**b**, **d**, **f**) of 20 vaccinated individuals (grey curves) and 8 control individuals (black curves). **a**, Anti-S IgG. **b**, Anti-RBD IgG. **c**, Anti-S IgM. **d**, Anti-RBD IgM. **e**, Anti-S IgA. **f**, Anti-RBD IgA. Left, optical density at 450 nm (OD 450 nm) for the indicated reciprocal plasma dilutions. Right, normalized AUC values for the 8 control and 20 vaccinated individuals. Horizontal bars indicate geometric mean. Statistical significance was determined using the two-tailed Mann–Whitney *U* test. Average of two or more experiments. **g**–**i**, Correlations of plasma antibody measurements. **g**, Normalized AUC for IgG anti-S (*x* axis) plotted against normalized AUC for IgG anti-RBD (*y* axis). **h**, Normalized AUC for IgM anti-S (*x* axis) plotted against normalized AUC for IgM anti-RBD (*y* axis). **i**, Normalized AUC for IgA anti-S (*x* axis) plotted against normalized AUC for IgA anti-RBD (*y* axis). The *r* and *P* values in **g**–**i** were determined with the two-tailed Spearman's correlation test. Individuals vaccinated with the Moderna vaccine are in black; individuals vaccinated with the Pfizer–BioNTech vaccine are in red. **j**–**l**, Results of ELISAs measuring plasma reactivity to RBD in volunteers who had recovered from COVID-19 at 1.3 and 6.2 months after infection[5,6] and in 20 vaccinated individuals, who received the Moderna vaccine (black dots) or Pfizer–BioNTech vaccine (red dots). **j**, Anti-RBD IgG. **k**, Anti-RBD IgM. **l**, Anti-RBD IgA. The normalized AUC values are shown. Positive and negative controls were included for validation. Red horizontal bars and indicated values represent geometric mean. Statistical significance was determined using two-tailed Mann–Whitney *U* test or Wilcoxon matched-pairs signed rank test.

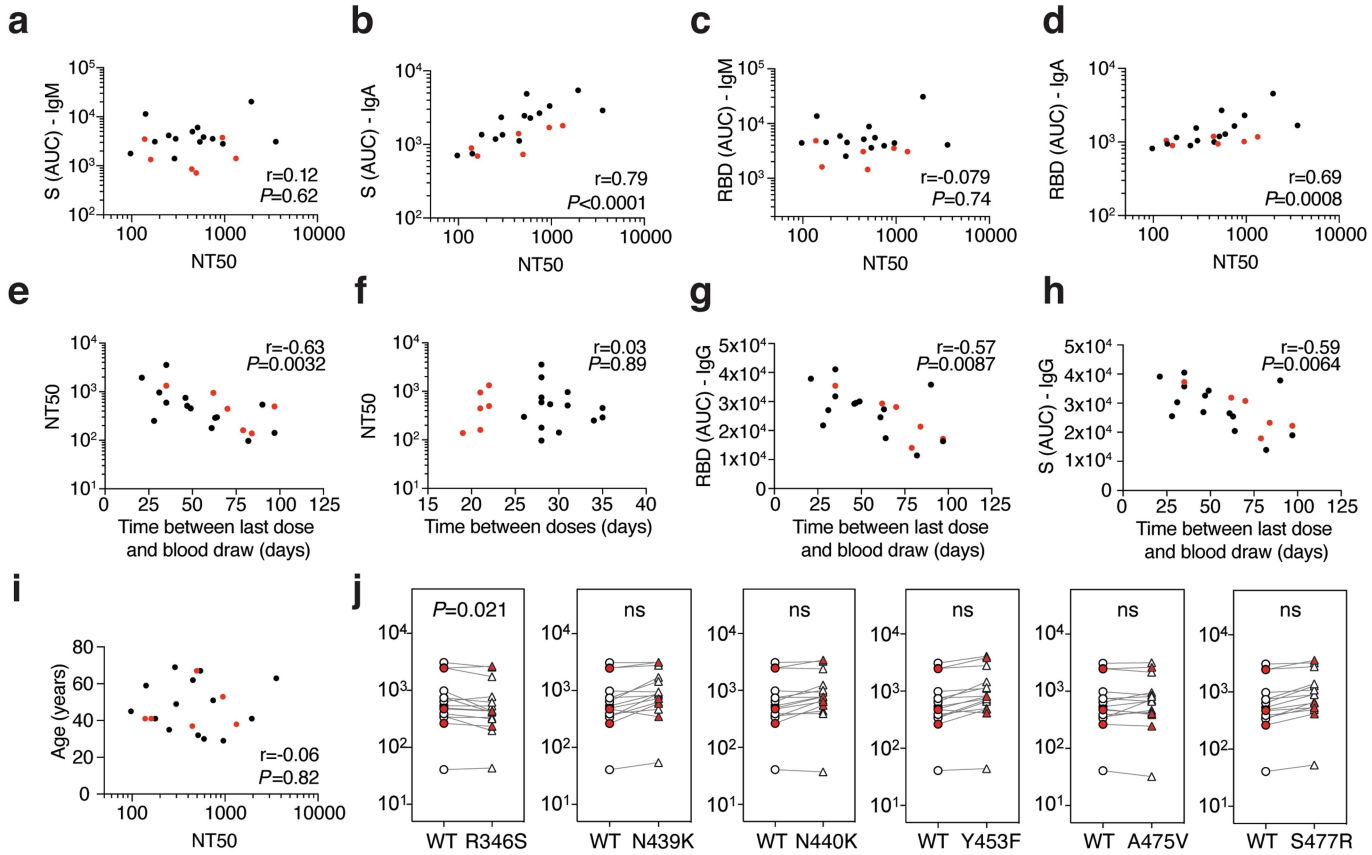

Extended Data Fig. 2 | Plasma neutralizing activity. a, Anti-S IgM AUC (*y* axis) plotted against NT_{50} (*x* axis). $r = 0.12$, $P < 0.62$. **b**, Anti-S IgA AUC (*y* axis) plotted against NT_{50} (*x* axis). $r = 0.79$, $P < 0.0001$. **c**, Anti-RBD IgM AUC (*y* axis) plotted against NT_{50} (*x* axis). $r = -0.079$, $P = 0.74$. **d**, Anti-RBD IgA AUC (*y* axis) plotted against NT_{50} (*x* axis). $r = 0.69$, $P = 0.0008$. **e**, NT_{50} (*y* axis) plotted against time between last dose and blood draw (*x* axis). $r = -0.63$, $P = 0.0032$. **f**, NT_{50} (*y* axis) plotted against time between doses (*x* axis). $r = 0.03$, $P = 0.89$. **g**, Anti-RBD IgG AUC (*y* axis) plotted against time between last dose and blood draw (*x* axis). $r = -0.57$, $P = 0.0087$. **h**, Anti-S IgG AUC (*y* axis) plotted against time between last dose and blood draw (*x* axis). $r = -0.59$, $P = 0.0064$. **i**, Age (*y* axis) plotted against NT_{50} (*x* axis). $r = -0.06$, $P = 0.82$. The *r* and *P* values were determined by two-tailed Spearman's. Individuals vaccinated with the Moderna vaccine are in black; individuals vaccinated with the Pfizer–BioNTech vaccine are in red. **j**, NT_{50} values for neutralization with plasma from vaccinated individuals ($n = 15$) of pseudotyped viruses with wild-type and the indicated RBD-mutant SARS-CoV-2 S. *P* values determined using one-tailed *t*-test.

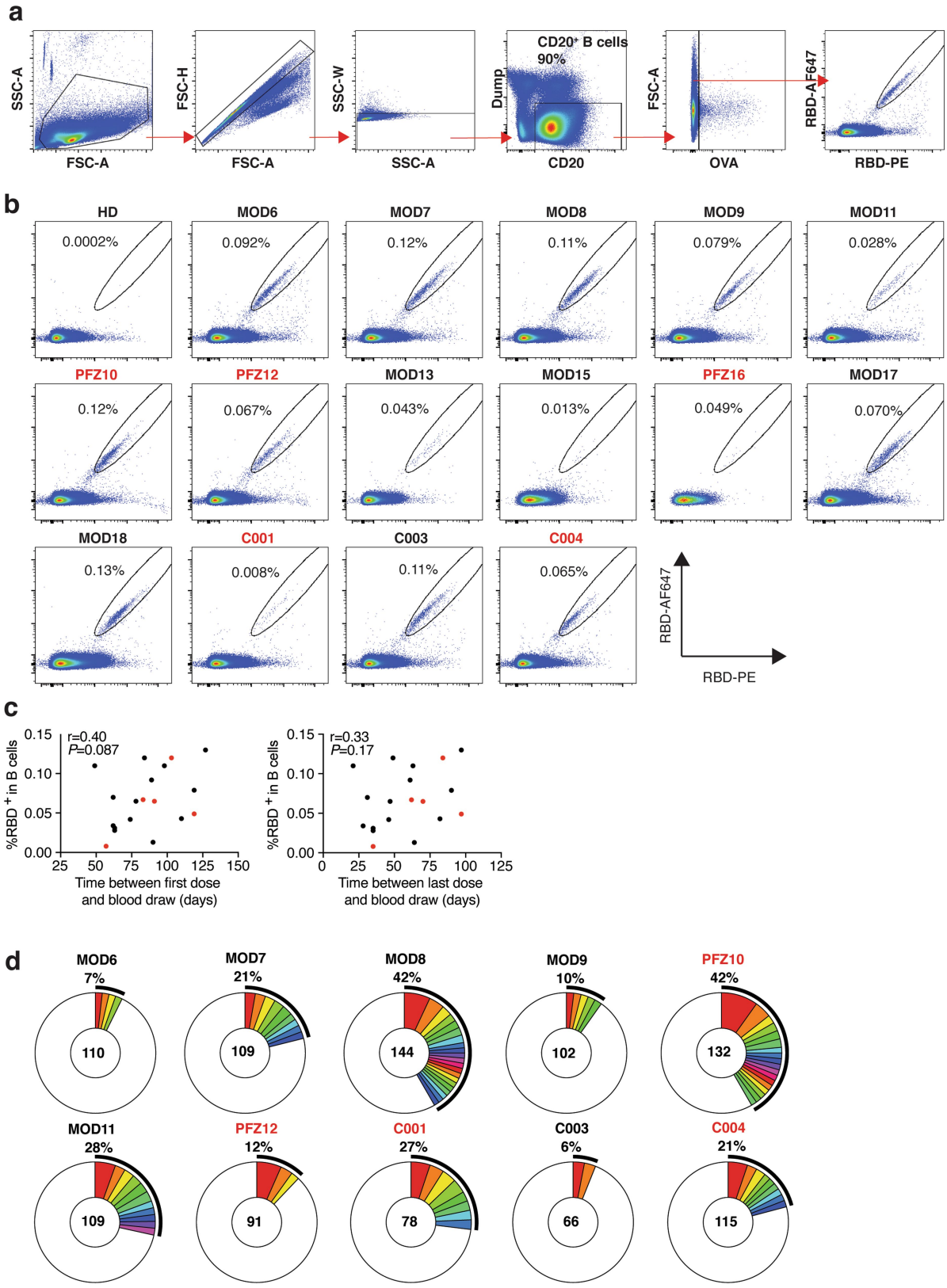

Extended Data Fig. 3 | See next page for caption.

Extended Data Fig. 3 | Flow cytometry. a, Gating strategy used for cell sorting. Gating was on singlets that were $CD20^+$ and $CD3^-CD8^-CD14^-CD16^-$ Iva^-. Sorted cells were $RBD\text{–}PE^+$ and $RBD\text{–}AlexaFluor647^+$. **b**, Flow cytometry showing the percentage of RBD-double-positive memory B cells from a pre-COVID-19 control (HD) and 15 vaccinated individuals, who received the Moderna vaccine (shown in black) or Pfizer–BioNTech vaccine (shown in red). **c**, The percentage of RBD-binding memory B cells in vaccinated individuals (*y* axis) plotted against time between first dose and blood draw (*x* axis) ($r = 0.40$, $P = 0.087$) (left) and between last dose and blood draw (*x* axis) ($r = 0.33$, $P = 0.17$) (right). Individuals vaccinated with the Moderna vaccine are in black; individuals vaccinated with the Pfizer–BioNTech vaccine are in red. The *r* and *P* values for correlations were determined by two-tailed Spearman's correlation test. **d**, Pie charts show the distribution of antibody sequences from ten individuals in **b**. The number in the inner circle indicates the number of sequences analysed. Pie-slice size is proportional to the number of clonally related sequences. The black outline indicates the frequency of clonally expanded sequences.

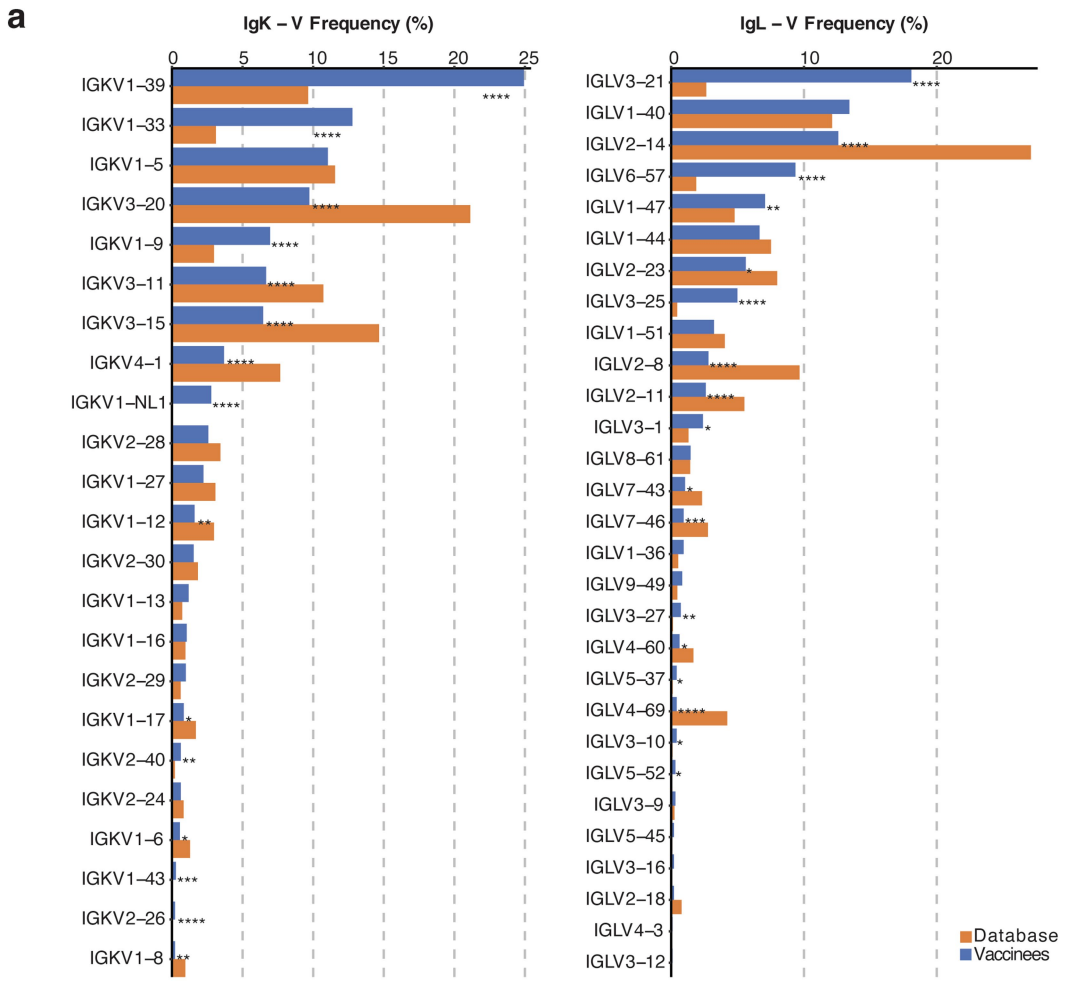

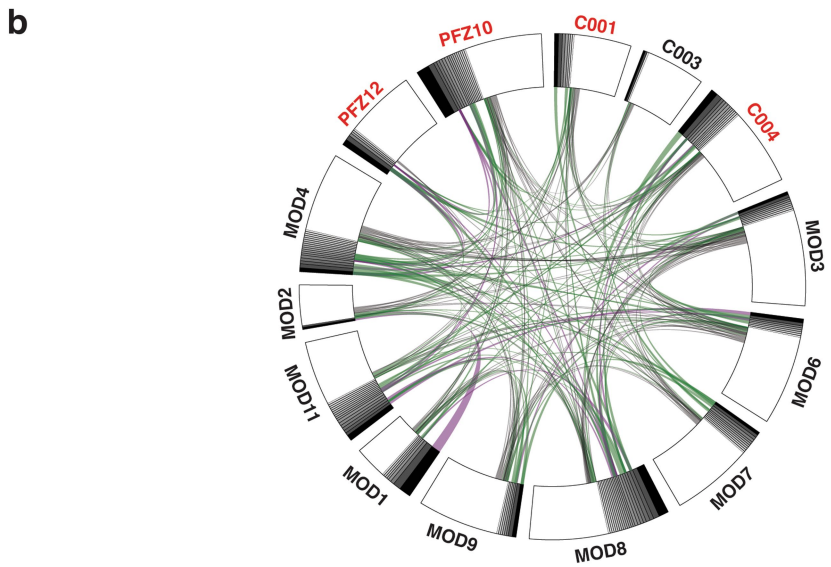

Extended Data Fig. 4 | Frequency distributions of human VL genes. Graph shows relative abundance of human IGVK (left) and IGVL (right) genes of Sequence Read Archive accession SRP010970 (database) (orange)[64], and vaccinated individuals (blue). Two-sided binomial tests with unequal variance were used to compare the frequency distributions. *$P < 0.05$, **$P < 0.01$, ***$P < 0.001$, ****$P < 0.0001$. **b**. Sequences from 14 individuals (Supplementary Table 3) with clonal relationships. Interconnecting lines indicate the relationship between antibodies that share V and J gene segment sequences at both IGH and IGL. Purple, green, and grey lines connect related clones, clones and singles, and singles to each other, respectively.

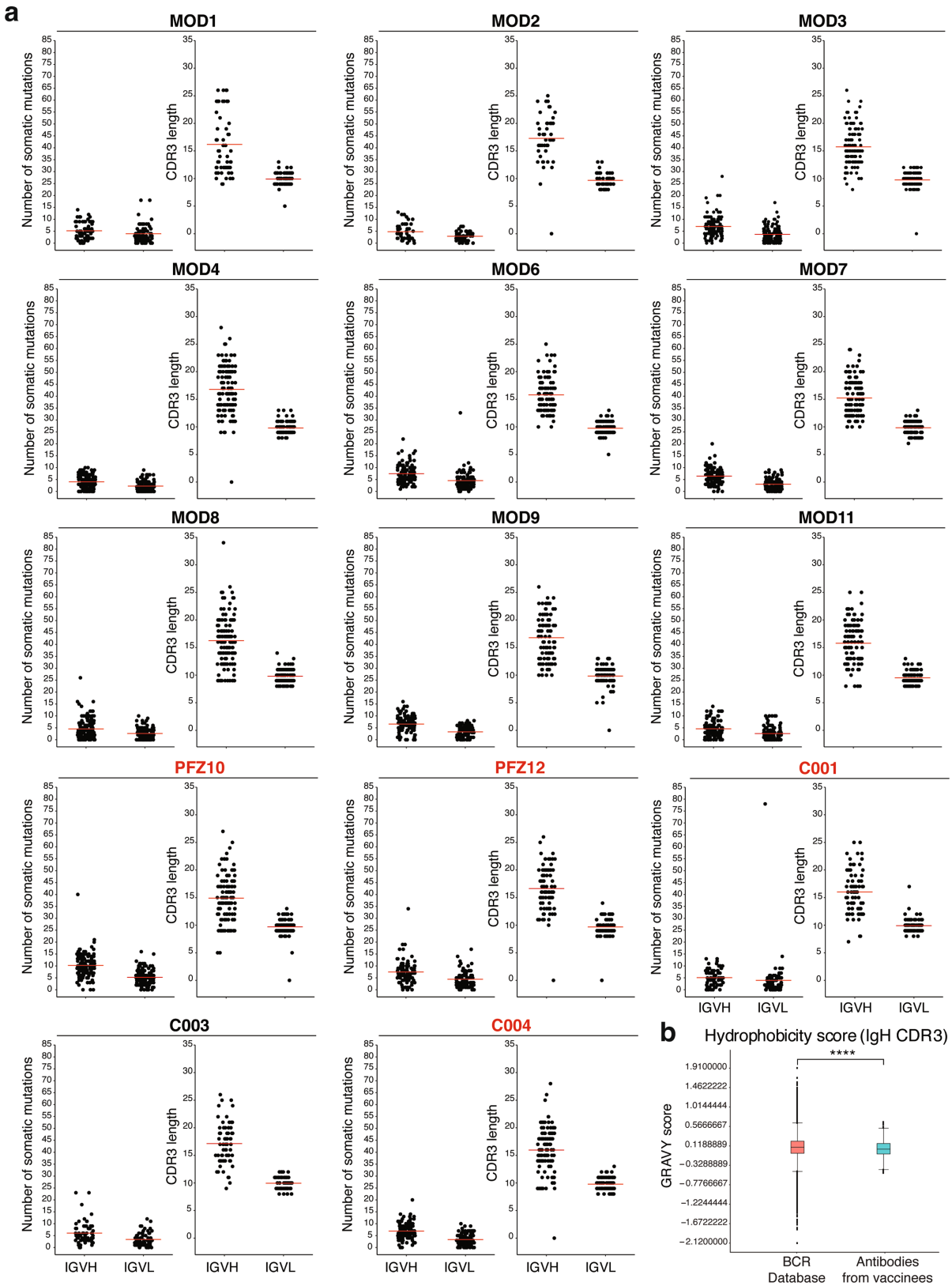

Extended Data Fig. 5 | Antibody somatic hypermutation, and CDR3 length. **a**, Number of somatic nucleotide mutations in both the IGVH and IGVL in 14 participants (left). Individuals who received the Moderna vaccine are shown in black, and individuals who received the Pfizer–BioNTech vaccine are shown in in red. For each individual, the number of amino acids in the CDR3 at the IGVH and IGVL is shown (right). The horizontal bars indicate the mean. The number of antibody sequences (IGVH and IGVL) evaluated for each participant are $n = 68$ (MOD1), $n = 45$ (MOD2), $n = 117$ (MOD3), $n = 123$ (MOD4), $n = 110$ (MOD6), $n = 109$ (MOD7), $n = 144$ (MOD8), $n = 102$ (MOD9), $n = 132$ (PFZ10), $n = 109$ (MOD11), $n = 91$ (PFZ12), $n = 78$ (C001), $n = 66$ (C003) and $n = 115$ (C004). **b**, Distribution of the hydrophobicity GRAVY scores at the IgH CDR3 compared to a public database (Methods). The box limits are the lower and upper quartiles, the centre line indicates the median, the whiskers are 1.5× interquartile range and the dots represent outliers. Statistical significance was determined using two-tailed Wilcoxon matched-pairs signed-rank test. ****$P < 0.0001$.

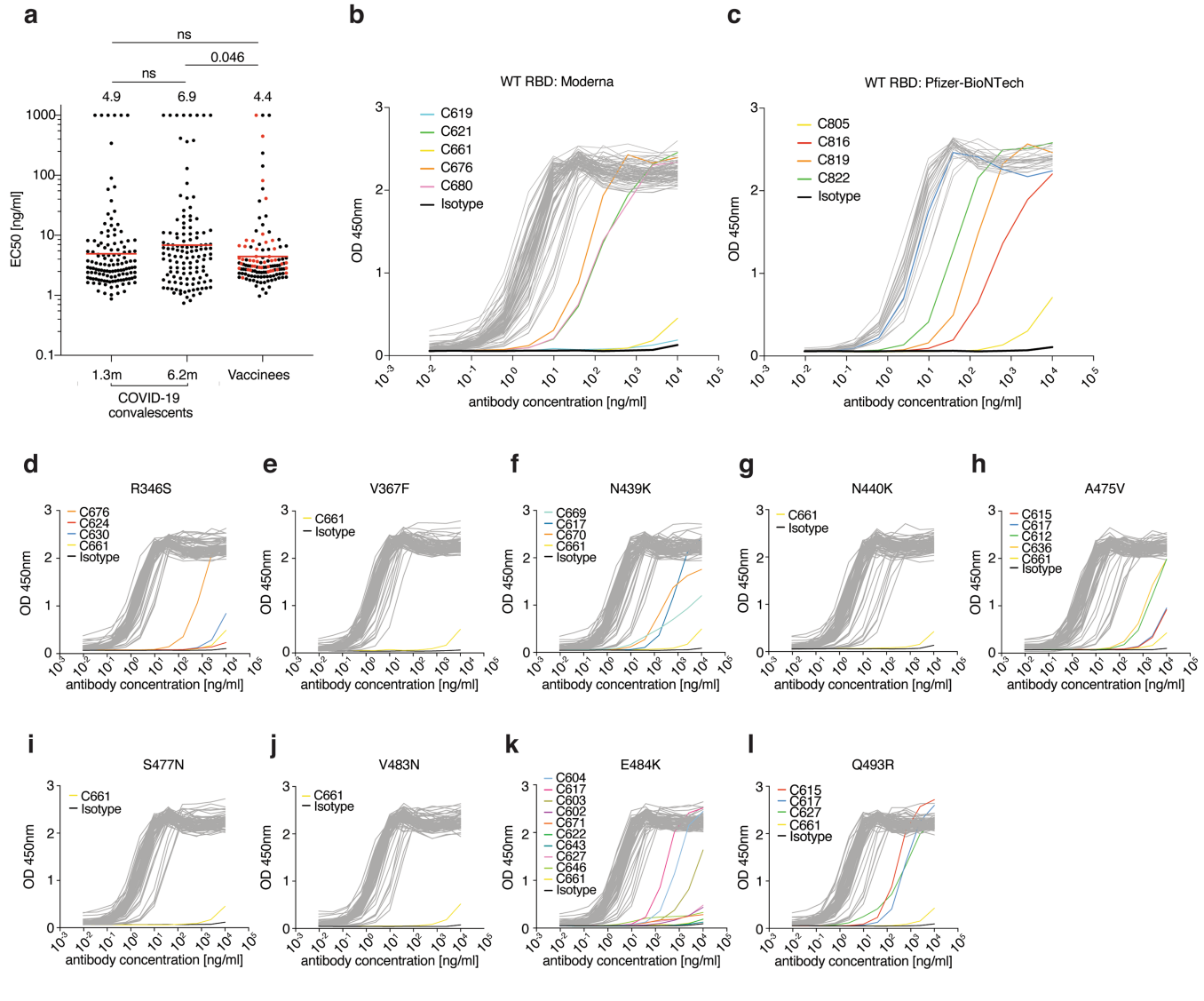

n

		WT	R346S	V367F	N439K	N440K	A475V	S477N	V483A	E484K	Q493R
Class 1	C682	2.4	2.2	2.6	3.6	3.5	35.0	3.3	2.8	3.7	4.1
	C613	2.0	1.9	1.8	3.3	2.5	126.1	2.4	2.3	2.2	4.9
	C663	1.9	1.8	1.7	2.7	2.5	12.6	2.3	2.0	2.4	2.2
	C614	1.4	1.6	1.6	2.0	1.9	2.5	1.8	1.9	1.6	1.8
	C660	2.0	2.0	2.1	2.3	2.7	2.5	2.1	2.2	2.4	2.2
Class 1/2	C653	2.1	2.1	2.1	2.5	2.6	2.2	2.1	2.3	4.0	3.1
Class 2	C627	1.6	1.6	1.8	2.0	2.0	2.1	1.9	1.8	1000	1000
	C602	2.0	1.8	1.9	2.1	2.2	2.2	2.1	3.1	1000	1.9
	C671	2.3	1.7	1.5	2.4	2.4	2.5	2.0	1.8	1000	2.5
	C643	2.1	2.2	2.3	2.0	2.2	1.7	1.8	2.5	1000	1.9
Class 2/3	C603	2.1	1.7	1.7	2.1	2.2	2.3	2.0	1.9	1000	1.9
	C628	2.7	1.9	2.0	4.3	3.2	3.1	2.4	2.4	10.0	3.2
Class 3	C669	2.3	2.1	2.2	950.6	291.8	2.1	2.1	2.2	2.4	2.2
	C670	2.9	2.1	2.3	210.7	2.8	3.0	2.6	2.4	3.3	3.3
Unclassified	C666	1.9	1.7	1.8	2.0	2.1	1.5	1.8	1.9	2.1	1.8
	C601	1.1	1.8	2.1	2.2	2.2	1.9	1.9	2.2	12.1	2.0
	C675	1.3	1.1	1.4	1.8	1.7	3.5	1.4	1.5	1.6	1.4

Extended Data Fig. 6 | See next page for caption.

Extended Data Fig. 6 | Monoclonal antibody ELISAs. a, Graphs show anti-SARS-CoV-2 RBD antibody reactivity. ELISA EC_{50} values for all antibodies isolated from individuals who had recovered from COVID-19 assayed at 1.3 and 6.2 months after infection[5,6] and 127 selected monoclonal antibodies isolated from 4 individuals who received the Moderna vaccine (black dots) and 4 who received the Pfizer–BioNTech vaccine (red dots), measured at 8 weeks after the boost. Red horizontal bars and indicated values represent geometric mean. Statistical significance was determined using two-tailed Mann–Whitney *U* test. **b**, **c**, Graphs show ELISA titration curves for 86 monoclonal antibodies isolated from individuals vaccinated with the Moderna vaccine (**b**) and 41 monoclonal antibodies isolated from individuals vaccinated with the Pfizer–BioNTech vaccine (**c**). **d**–**l**, Graphs show ELISA titrations for 84 antibodies isolated from individuals vaccinated with the Moderna vaccine against the indicated RBD variants. Isotype control and low-binding antibodies are indicated in colours. C661 is a nonbinding antibody. Data are representative of two independent experiments. **m**, Relative change in EC_{50} values for the indicated RBD variants over wild-type RBD of 84 antibodies isolated from individuals vaccinated with the Moderna vaccine. Red horizontal bars represent geometric mean. **n**, Heat-map summary of EC_{50} values for binding to wild-type RBD and the indicated mutant RBDs for 17 top neutralizing antibodies.

a

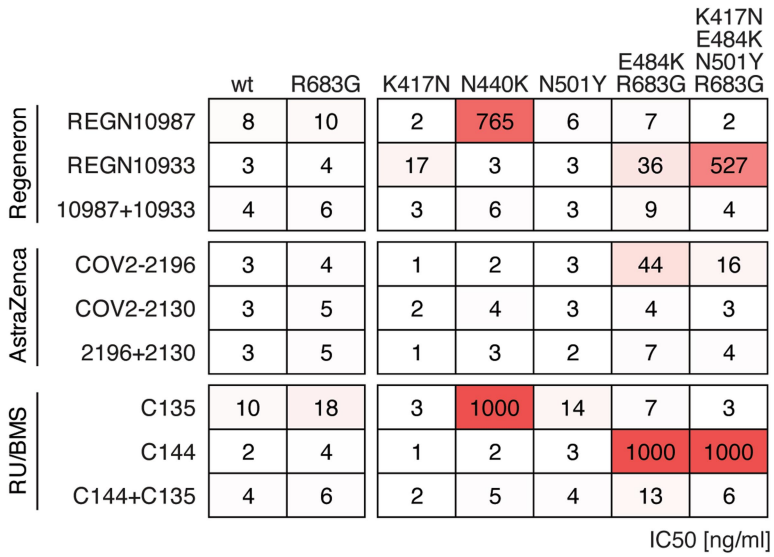

Extended Data Fig. 7 | Neutralizing activity of monoclonal antibodies in clinical development against SARS-CoV-2 variants. Results of a SARS-CoV-2 pseudovirus neutralization assay. IC_{50} values for six different monoclonal antibodies, alone or in their clinically designated combinations, for neutralization of wild-type and the indicated mutant SARS-CoV-2 pseudotyped viruses. Antibodies with IC_{50} values above 1,000 ng ml^{-1} are plotted as 1,000 ng ml^{-1}. Data are the mean of two independent experiments. Colour gradient indicates IC_{50} values, ranging from 0 (white) to 1,000 ng ml^{-1} (red). The combination of REGN10987 and REGN10933 (casirivimab and imdevimab, respectively)[14,65,66] has been granted emergency use authorization by the US Food and Drug Administration; the combination of COV2-2196 and COV2-2130 (licensed to AstraZeneca as AZD7442)[27] and the combination of C135 and C144 (Rockefeller University)[6] are currently in clinical trials (NCT04507256 and NCT04700163, respectively).

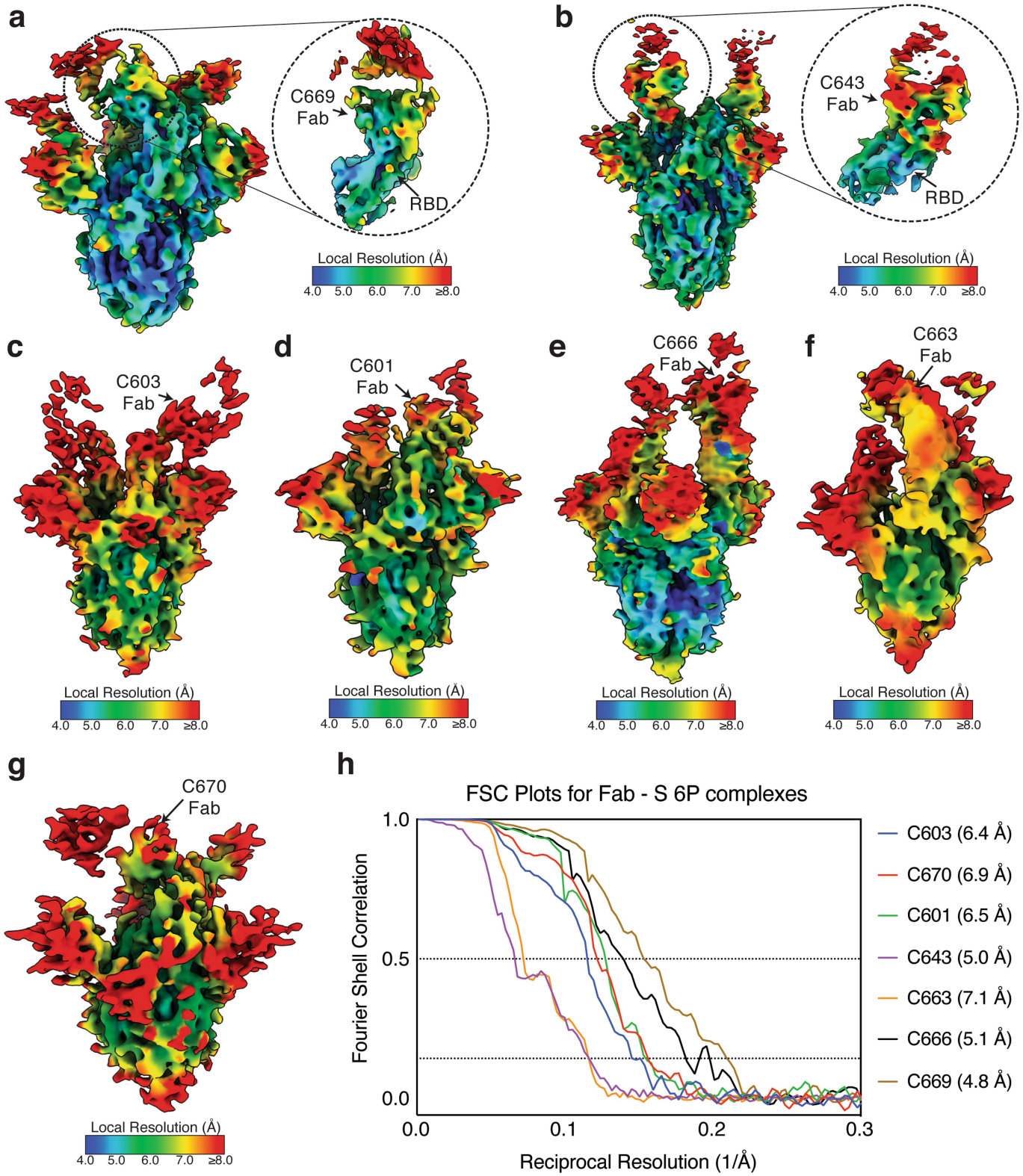

Extended Data Fig. 8 | Local resolution estimates of Fab–S cryo-EM reconstructions. a–g, Local-resolution maps calculated using cryoSPARC for C669–S (**a**), C643–S (**b**), C603-S (**c**), C601–S (**d**), C666–S (**e**), C663–S (**f**) and C670–S (**g**) complexes. Close-up views for Fab–RBD interfaces are highlighted for C669 (**a**) and C643 (**b**). **h**, Gold-standard Fourier shell correlation curves for Fab–S complexes. The 0.5 and 0.143 cut-offs are indicated by dashed lines.

nature research

Corresponding author(s): Theodora Hatziioannou,Rafael Casellas, Paul Bieniasz, Pamela J. Bjorkman, Michel Nussenzweig

Last updated by author(s): Feb 1st, 2021

Reporting Summary

Nature Research wishes to improve the reproducibility of the work that we publish. This form provides structure for consistency and transparency in reporting. For further information on Nature Research policies, see Authors & Referees and the Editorial Policy Checklist.

Statistics

For all statistical analyses, confirm that the following items are present in the figure legend, table legend, main text, or Methods section.

n/a	Confirmed
☐	☒ The exact sample size (*n*) for each experimental group/condition, given as a discrete number and unit of measurement
☐	☒ A statement on whether measurements were taken from distinct samples or whether the same sample was measured repeatedly
☐	☒ The statistical test(s) used AND whether they are one- or two-sided *Only common tests should be described solely by name; describe more complex techniques in the Methods section.*
☒	☐ A description of all covariates tested
☒	☐ A description of any assumptions or corrections, such as tests of normality and adjustment for multiple comparisons
☒	☐ A full description of the statistical parameters including central tendency (e.g. means) or other basic estimates (e.g. regression coefficient) AND variation (e.g. standard deviation) or associated estimates of uncertainty (e.g. confidence intervals)
☐	☒ For null hypothesis testing, the test statistic (e.g. *F*, *t*, *r*) with confidence intervals, effect sizes, degrees of freedom and *P* value noted *Give P values as exact values whenever suitable.*
☒	☐ For Bayesian analysis, information on the choice of priors and Markov chain Monte Carlo settings
☒	☐ For hierarchical and complex designs, identification of the appropriate level for tests and full reporting of outcomes
☒	☐ Estimates of effect sizes (e.g. Cohen's *d*, Pearson's *r*), indicating how they were calculated

Our web collection on statistics for biologists contains articles on many of the points above.

Software and code

Policy information about availability of computer code

Data collection	IRIS by iMedRIS version 11.01 for clinical data collection and management; BD FACSDiva Software Version 8.0.2 for flow sorting; Glomax Navigator Promega V.3 for neutralization assays; Omega 5.11 by BMG Labtech was used for Elisa Assays, Illumina Miseq, SerialEM automated image acquisition software version 3.7.
Data analysis	FlowJo 10.6.2 for FACS analysis; GraphPad Prism 8.4; Microsoft Excel 16.36; MacVector 17.5.4 for sequence analysis; Omega MARS V2.10 by BMG Labtech for luminometer; Glomax Navigator V.3 from Promega, Adobe Illustrator 2020, Geneious Prime (Version 2020.1.2), cryoSPARC v2.15 and UCSF chimera version 1.13.1 for EM analysis; BBDuk for sequencing read processing, scripts and the data used to process antibody sequences are available on GitHub (https://github.com/stratust/igpipeline).

For manuscripts utilizing custom algorithms or software that are central to the research but not yet described in published literature, software must be made available to editors/reviewers. We strongly encourage code deposition in a community repository (e.g. GitHub). See the Nature Research guidelines for submitting code & software for further information.

Data

Policy information about availability of data

All manuscripts must include a data availability statement. This statement should provide the following information, where applicable:

- Accession codes, unique identifiers, or web links for publicly available datasets
- A list of figures that have associated raw data
- A description of any restrictions on data availability

Data are provided in SI Table 3-5 and 7. The raw sequencing data and computer scripts associated with Figure 2 has been deposited at Github (https://github.com/stratust/igpipeline). This study also uses data from "A Public Database of Memory and Naive B-Cell Receptor Sequences" (https://doi.org/10.5061/dryad.35ks2), PDB (6VYB and 6NB6) and from "High frequency of shared clonotypes in human B cell receptor repertoires" (https://doi.org/10.1038/s41586-019-0934-8). Cryo-EM maps associated with data reported in this manuscript will be deposited in the Electron Microscopy Data Bank (EMDB: https://www.ebi.ac.uk/pdbe/emdb/) under accession codes EMD-23393 (C601-S), EMD-23394 (C603-S), EMD-23395 (C643-S), EMD-23396 (C663-S), EMD-23397 (C666-S), EMD-23398 (C669-S), and

EMD-23399 (C670-S).

Field-specific reporting

Please select the one below that is the best fit for your research. If you are not sure, read the appropriate sections before making your selection.

☒ Life sciences ☐ Behavioural & social sciences ☐ Ecological, evolutionary & environmental sciences

For a reference copy of the document with all sections, see nature.com/documents/nr-reporting-summary-flat.pdf

Life sciences study design

All studies must disclose on these points even when the disclosure is negative.

Sample size	Sample size of 20 individuals was based on succesful recruitment of volunteers who received two doses of the Moderna or Pfizer mRNA vaccines between 19 October 2020 and 15 January 2021.
Data exclusions	No data were excluded from the analysis.
Replication	All experiments successfully repeated at least twice.
Randomization	This is not relevant as this is an observational study.
Blinding	This is not relevant as this is an observational study.

Reporting for specific materials, systems and methods

We require information from authors about some types of materials, experimental systems and methods used in many studies. Here, indicate whether each material, system or method listed is relevant to your study. If you are not sure if a list item applies to your research, read the appropriate section before selecting a response.

Materials & experimental systems

n/a	Involved in the study
☐	☒ Antibodies
☐	☒ Eukaryotic cell lines
☒	☐ Palaeontology
☒	☐ Animals and other organisms
☐	☒ Human research participants
☒	☐ Clinical data

Methods

n/a	Involved in the study
☒	☐ ChIP-seq
☐	☒ Flow cytometry
☒	☐ MRI-based neuroimaging

Antibodies

Antibodies used	Mouse anti-human CD20-PECy7 (BD Biosciences, 335793), clone L27 Mouse anti-human CD3-APC-eFluro 780 (Invitrogen, 47-0037-41), clone OKT3 Mouse anti-human CD8-APC-421eFluro 780 (Invitrogen, 47-0086-42), clone OKT8 Mouse anti-human CD16-APC-eFluro 780 (Invitrogen, 47-0168-41), clone eBioCB16 Mouse anti-human CD14-APC-eFluro 780 (Invitrogen, 47-0149-4), clone 61D3 Zombie NIR (Biolegend, 423105) Peroxidase Goat anti-Human lgG Jackson Immuno Research 109-036-088 Peroxidase Goat anti-Human lgM Jackson Immuno Research 109-035-129 Peroxidase Goat anti-Human lgA Sigma A0295
Validation	No validation statements for the antibodies that are commercially available.

Eukaryotic cell lines

Policy information about cell lines

Cell line source(s)	293T (ATCC CRL-11268) 293T / ACE2.cl22 HT1080/ACE2.cl14 (Schmidt, F. et al. J Exp Med 217, doi:10.1084/jem.20201181)
Authentication	Not authenticated after purchase from ATCC.

Mycoplasma contamination	The cells were checked for mycoplasma contamination by Hoechst staining.
Commonly misidentified lines (See ICLAC register)	No commonly misidentified cell lines were used.

Human research participants

Policy information about studies involving human research participants

Population characteristics	A cohort of 20 individuals that participated in either the Moderna or Pfizer phase 3 vaccine clinical trial was recruited at the NIH Blood Center and the Rockefeller University Hospital for blood donation. Eligible participants included adults, at least 18 years of age with no known heart, lung, kidney disease or bleeding disorders, no history of HIV-1 or malaria infection. All participants were asymptomatic at the time of the study visit and had received a complete 2 dose regimen of either mRNA vaccine. Informed consent was obtained from all participants and the study was conducted in accordance with Good Clinical Practice. The study visits and blood draws were reviewed and approved under the National Institutes of Health's Federalwide Assurance (FWA00005897), in accordance with Federal regulations 45 CFR 46 and 21 CFR 5 by the NIH Intramural Research Program IRB committee (IRB# 99CC0168, Collection and Distribution of Blood Components from Healthy Donors for In Vitro Research Use) and by the Institutional Review Board of the Rockefeller University (IRB# DRO-1006, Peripheral Blood of Coronavirus Survivors to Identify Virus-Neutralizing Antibodies).
Recruitment	Between 19 October 2020 and 15 January 2021, 20 volunteers who received two doses of the Moderna (n=14) or Pfizer mRNA (n=6) vaccines were recruited for blood donation and analyzed. Ages of the analyzed volunteers ranged from 29-69 years (median 43); 12 (60%) were male and 8 (40%) female. 16 participants identified as Caucasian, 2 as Hispanic, and 1 as African American or Asian, respectively. The time from the second vaccination to sample collection varied between 3-14 weeks with an average of 8 weeks. None of the volunteers had a history of prior SARS-CoV-2 infection and none reported serious adverse events after vaccination
Ethics oversight	NIH Intramural Research Program IRB committee (IRB# 99CC0168, Collection and Distribution of Blood Components from Healthy Donors for In Vitro Research Use) and by the Institutional Review Board of the Rockefeller University (IRB# DRO-1006, Peripheral Blood of Coronavirus Survivors to Identify Virus-Neutralizing Antibodies)

Note that full information on the approval of the study protocol must also be provided in the manuscript.

Flow Cytometry

Plots

Confirm that:

☒ The axis labels state the marker and fluorochrome used (e.g. CD4-FITC).

☒ The axis scales are clearly visible. Include numbers along axes only for bottom left plot of group (a 'group' is an analysis of identical markers).

☒ All plots are contour plots with outliers or pseudocolor plots.

☒ A numerical value for number of cells or percentage (with statistics) is provided.

Methodology

Sample preparation	Whole blood samples were obtained from study participants recruited through NIH or Rockefeller University Hospital. Peripheral blood mononuclear cells (PBMCs) were separated by Ficoll gradient centrifugation. Prior to sorting, PBMCs were enriched for B cells using a Miltenyi Biotech pan B cell isolation kit (cat. no. 130-101-638) and LS columns (cat. no. 130-042-401).
Instrument	FACS Aria III (Becton Dickinson)
Software	BD FACSDiva Software Version 8.0.2 and FlowJo 10.6.2
Cell population abundance	Sorting efficiency ranged from 24% to 77%. This is calculated based on the number of IgG-specific antibody sequences that could be PCR-amplified successfully from single sorted cells from each donor.
Gating strategy	Cells were first gated for lymphocytes in FSC-A (x-axis) versus SSC-A (y-axis). We identify single cells in FSC-A versus FSC-H, and then SSC-A versus SSC-W. We then select for CD20+ Dump- B Cells in dump (anti-CD3-eFluro 780, anti-CD16-eFluro 780, anti-CD8-eFluro 780, anti-CD14-eFluro 780, Zombie NIR) versus CD20 (anti-CD20-PE-Cy7); dump-negative was considered to be signal less than 250, and CD20-positive was taken to be signal greater than 100. We then gate for Ova- B cells in FSC-A versus Ova-BV711; Ova-negative was considered to be all cells with signal less than 100. Select for Sars-CoV-2 RBD double positive cells in RBD PE versus RBD Alexa Fluor 647; this gate was made along the 45 diagonal, above 103 on both axes.

☒ Tick this box to confirm that a figure exemplifying the gating strategy is provided in the Supplementary Information.